OceanICU
Understanding Ocean Carbon

Deliverable D5.2

Summary of material passed to WP 7

27-08-2025/v1.0

OceanICU was funded by the European Union under grant agreement no. 101083922 and UK Research and Innovation (UKRI) under the UK government's Horizon Europe funding guarantee [grant number 10054454, 1006367, 10064020, 10059241, 10079684, 10059012, 10048179]. Views and opinions expressed are however those of the author(s) only and do not necessarily reflect those of the European Union or European Research Executive Agency. Neither the European Union nor the granting authority can be held responsible for them

UK Research and Innovation

About this document

Title	D5.2, Summary of material passed to WP7
Work Package	WP5, Impacts of Fishing and Industrial Extraction processes on the Ocean C cycle
Lead Partner	DTU, GEOMAR
Lead Author (Org)	Ken H. Andersen (DTU), Matthias Haeckel (GEOMAR)
Contributing Author(s)	Matthias Haeckel (GEOMAR) Ken H. Andersen (DTU) Paula Silvar (MI) Patrick Lehodey (MOI) Dougie Speirs (UStrath) Emma Dolmaire (UStrath) Mike Heath (UStrath) Maximilien Cosme (Agrocampus) Karline Soetaert (NIOZ)
Reviewers	Richard Sanders, NORCE
Due Date	31.08.2025, M34
Submission Date	27.08.2025
Version	**1.0**

Dissemination Level

x	PU: Public – fully open (automatically posted online)
	SEN: Sensitive – limited under the conditions of the Grant Agreement

OceanICU: Improving Carbon Understanding is a Research and Innovation action (RIA) funded by the Horizon Europe Work programme topics addressed: HORIZON-CL6-2022-CLIMATE-01-02. Start date: 01 November 2022. End date: 31 October 2027.

Funded by the European Union

UK Research and Innovation

This work was funded by the European Union under grant agreement no. 101083922 (OceanICU) and UK Research and Innovation (UKRI) under the UK government's Horizon Europe funding guarantee [grant number 10054454, 10063673, 10064020, 10059241, 10079684, 10059012, 10048179]. Views and opinions expressed are however those of the author(s) only and do not necessarily reflect those of the European Union or European Research Executive Agency. Neither the European Union nor the granting authority can be held responsible for them.

Contents

Key messages for the Ocean ICU stakeholders

Not applicable

Abstract

This deliverable describes the first set of data passed to WP7 for using in developing fast DST model simulations. We have focused on data sets on the human interventions that we expect have the biggest impact on the respective ecosystems. Based on the response from WP7 we can then target more simulations better suited towards their need.
The deliverable involves work in tasks 5.1 to 5.4: impacts of deep-seabed mining and drilling activities on the open ocean, impacts of sediment-generating (e.g. dredging, trawling) activities on the shelf-sea ecosystems, impacts of fishing on carbon sequestration in the on-shelf ecosystem, and impacts of fishing on carbon sequestration in the off-shelf ecosystem.

Work carried out

In the following we introduce each task (using text from D5.1) and outline the specific question addressed with each model.

Task 5.1: Impacts of deep seabed mining and drilling activities on the open ocean

In Task 5.1 we have identified that impacts of deep-sea mining activities are expected to have larger spatial footprints in the marine environment than other industrial processes, such as dredging and drilling. Since the International Seabed Authority (ISA) is currently drafting the regulation for the exploitation of mineral resources, closing scientific knowledge gaps of impacts from deep-sea mining is also a priority in marine policy. Therefore, we have decided to focus our work on this industrial activity, and in particularly the mining of polymetallic nodules (PMN), it will create a spatially larger environmental footprint than the mining of seafloor massive sulfides (SMS) and Co-rich ferromanganese crusts (CRC).

For economic reasons companies interested in deep-sea mining expect that they need to mine 2-3 Mio t dry weight of PMN per year and mining operation. In economically interesting areas, such as the Clarion-Clipperton Zone (CCZ) in the NE equatorial Pacific, where the ISA has issued 18 exploration contracts until today, this equates to an area of about 200 km^2 per year and mining operation. Current technology for mining of PMN will remove together with the resource also the entire bioturbated layer of the seafloor sediments,

including its epi- and endofauna. The main fraction of the removed sediments is suspended into the bottom water at the back of the vehicle and disperses driven by its own density-driven hydrodynamics and the bottom currents. An additional sediment plume is created in the water column by the discharge from the surface platform after cleaning of the nodules from remaining sediment. The largest fraction of the suspended sediments will sink to the seafloor, where it will blanket the habitat, thereby impacting an additional area outside the mined area. First data on the resulting impacts on the marine environment and the behaviour of the suspended sediment plume are available from the MiningImpact project, which collected data in connection with the first industrial test of a collector vehicle in the CCZ. Some additional information was produced in connection of benthic impact experiments conducted more than 25 years ago and that have been revisited during the MiningImpact project.

Specific questions addressed

In Task 5.1 we addressed mining-induced impacts on benthic and pelagic biogeochemical processes separately. A sediment biogeochemical model (C.CANDI) was applied to quantify the change of carbon remineralization and burial (i.e. storage) below the bioturbated zone, whereas the pelagic biogeochemical model MOPS (Model of Oceanic Pelagic Stoichiometry) within the framework FABM (The Framework for Aquatic Biogeochemical Models) coupled to the 1D physical host model GOTM (General Ocean Turbulence Model) was applied to simulate scenarios for impacts of waste sediment material injected into different water depths to identify respective model parameter sensitivities affecting carbon production, remineralization and export to the seafloor.

With MOPS we specifically analyzed the effects of increased particle loads in the water column on five different processes: (1) an increased light attenuation coefficient, κ_{sed}, on the growth of phytoplankton; (2) a reduced maximum grazing rate of zooplankton species, μ_{zoo}, being able to discriminate nutrients from sediment particles, but leading to more difficult access to nutrients or escape reactions; (3) a reduced food assimilation rate of zooplankton, ε_{zoo}, eating everything (e.g. nutritional values are decreased, clogging of gut tract); (4) a decreased density-dependent loss rate of zooplankton, κ_{zoo}, representing the effect on higher-trophic level fauna (e.g. fish); and (5) an increased zooplankton mortality, λ_{zoo}, due to potential toxicity of particles and stress effects. Due to lack of knowledge of elevated particle loads from deep-sea mining activities and largely also on respective effects on deep-sea organisms, these response types were identified from available literature on shallow water organisms and non-open-ocean environments (e.g., van der Grient and Drazen, 2022). Another effect, the flocculation and aggregation of particles

and potentially increased export to the seafloor, has not yet been implemented in the model.

With C.CANDI we simulated the consequences of surface sediment removal during PMN collection on the benthic organic carbon remineralization by microbes. The simulations followed our previous studies (König et al., 2001; Haffert et al., 2020; Volz et al., 2020), which were now underpinned by first data gained from the monitoring of a nodule collector test in the Clarion-Clipperton Zone (Vink, 2022). The key biogeochemical variable in this context are dissolved oxygen micro-profiles measured in situ in the sediment in the mined area.

Task 5.2: Impacts of sediment generating (e.g. dredging, trawling) activities on the shelf sea ecosystems

Shelf-sea sediments harbour significant levels of biodiversity that play a key role in ecosystem functions and services such as biogeochemical cycling, and carbon storage. Bioturbation and bioirrigation, the faunal activity that results in particle displacement and increased exchange of solutes (e.g. CO_2) across the sediment-water interface and within the sediment matrix, has a large impact on the degradation of organic matter into inorganic bioavailable forms and thus on carbon sequestration.

In addition to directly changing the sediment biogeochemistry, bottom disturbing activities also remove benthic organisms and change the species composition. This alters the functional traits in terms of bioturbation and bio-irrigation of a community, which in turn may have broad implications for the overall biogeochemical functioning of the sediment.

To include this biological-biogeochemical interaction, our impact assessment couples a biological and biogeochemical model:

In (i) the *biological* part, a data-driven mechanistic model is used to describe species depletion during and recovery between trawling events. As the species densities change due to trawling, so do the bioturbation and bio-irrigation activity performed by the biological community. This has impact on (ii) the *biogeochemical* model, which is an early diagenetic model, based on OMEXDIA. Upon trawling, the sediment and organic matter in this model is mixed and partly resuspended, while porewater with nutrients, and organic carbon is lost to the overlying water column.

First results on the biological part are available, and steps have been taken to couple this to the biogeochemical model.

Task 5.3: Impacts of fishing on carbon sequestration in shelf ecosystem

Task 5.3 examines the role of fishing on carbon sequestration in shelf seas using three modelling systems:

The first is **StrathE2E**. StrathE2E is a marine food web model of intermediate complexity which represents a spatially aggregated shelf sea region. The model simulates the fluxes of nutrient (nitrogen) through the ecosystem from dissolved inorganic (nitrate and ammonia), through plankton, benthos and fish, to birds and mammals, its regeneration through excretion and mineralization of detritus in the water column and sediment, and the physical oceanographic, land-sea, and air-sea exchanges across the geographic boundaries. The model will be adapted to translate Nitrogen to Carbon in as much as is feasible. It will be used to explore a range of fishing and environmental scenarios including climate change and changes in fishing. StrathE2E is used in the Celtic Sea.

The second model used is **Ecopath with Ecosim** (EwE). Ecopath is an ecological/ecosystem modelling software suite. EwE has three main components: Ecopath – a static, mass-balanced snapshot of the system; Ecosim – a time dynamic simulation module for policy exploration; and Ecospace – a spatial and temporal dynamic module primarily designed for exploring impact and placement of protected areas. Ecopath is designed as a model to investigate fishery and food web interactions, but will be modified to include the carbon budget aspects of fishing on the ecosystem and food web. Again, this will then be used to explore the same scenarios as will be used in StrathE2E. To setups of EwE are used in the Irish Sea

The third modelling approach uses **EcoTroph**. EcoTroph (ET) is articulated around the idea that an ecosystem can be represented by its biomass distribution across trophic levels, the biomass trophic spectrum. The ecosystem functioning is viewed as a biomass flow moving from lower to higher trophic levels, due to predation and ontogenetic processes. Thus, the ecosystem biomass present at a given trophic level may be estimated from two simple equations, one describing biomass flow, the other their kinetics (which quantifies the velocity of biomass transfers towards top predators). Again, this will be used to explore scenarios of climate change and fishing and the potential impacts on carbon sequestration.

The key common factor for these three modelling approaches is that the great bulk of fishing actually occurs in shelf seas, and not the open ocean. But the understanding of the functioning of the BCP is much less well developed than for the open ocean. Water column attenuation of deadfall or faeces will be much less important in these relatively shallow waters. This biological material will also enter the benthic food web where there are many detritivores, in contrast to the deep sea. Finally, the shelf sea sediments are subject to much

greater disturbance, and hence possible remineralisation than are the deep ocean sea-beds. This disturbance includes: water movement e.g. currents, tides and turbulence; bioturbation by benthic infauna; and anthropogenic disturbance, predominantly fishing. The aim will be to use these models to help quantify carbon flux, identify the relative importance of that in a local and global scale, and identify how fishing would be expected to perturb that flux and pathway to sequestration.

Task 5.4: Impacts of deep seabed mining and drilling activities on the open ocean

Task 5.4 examines the role of fishing on carbon sequestration in the off-shelf sea. This work is focused on potential fishing for large pelagic fish. This task uses two modelling systems:

The first model is the **Spatial Ecosystem and Population Dynamics Model – SEAPODYM**. This is a numerical model developed for investigating physical-biological interactions between fish populations and the ocean pelagic ecosystem. The focus of this work in OceanICU is on actual current fishing for small and large pelagic fish (e.g. mackerel and tuna respectively), and will examine both direct carbon aspects, as in the removal of biomass, and indirect effects via the food web interactions.

The second model system is **FEISTY**, which is a temporally dynamic, spatially explicit, mechanistic model of size-structured forage, large pelagic, and demersal fish functional types and an unstructured benthic invertebrate biomass pool. Fish functional types are defined by their maximum size, habitat, and prey preference.

We focus on the impact of fishing only on the large pelagic species. This would typically be fishing on scombroids (tuna etc) in equatorial upwelling. These fisheries are some of the biggest world-wide with an annual catch in the order of 3 M tonnes. We expect that fishing on the large pelagic fish will have two effects on carbon sequestration: First, fishing reduces the stocks and thereby the flux of fecal pellets that are released. This will lead to a reduction in carbon sequestration. Second, the reduction of the large pelagic fish will lead to a diminished predation pressure on small pelagic and mesopelagic fish. This release of predation will lead to an *increase* in stocks of small fish and consequently an increase in fecal pellets and carbon sequestration. Further, as small fish have a faster metabolism than the large pelagic fish the increased carbon sequestration could potentially more than outweigh the reduced carbon sequestration due to the direct effect of fishing on large pelagic fish. As a measure of potential changes in the carbon sequestration we focus here on the flux of fecal pellets to the seabed.

The question that we address is therefore:

What is the carbon flux to the seabed under fishing vs. no fishing?

Main results achieved

In the following we describe the results of simulations performed and describe the provided data set.

Task 5.1: Impacts of deep seabed mining and drilling activities on the open ocean

Pelagic simulations were carried out for the location of the German PMN license area of BGR in the Clarion-Clipperton Zone in the NE equatorial Pacific. The FABM-MOPS parameter sensitivity experiments considered five different hypothetical injection depths (65, 225, 1150, 2450, and 4050 m) and four discharge times (1, 4, 8, 26 weeks) at a sediment discharge rate of 1.2 kg/s, equivalent to about 10% of the seafloor sediment mass removal (Gazis et al., 2025). Table 5.1.1 provides an overview of the ensemble of parameter settings.

Due to the implicit assumption of the physical 1D host model GOTM to be horizontally homogeneous, we also needed to assume an initial area for the model box of the sediment discharge plume. We defined it as the horizontal extent where the moving plume source becomes neutrally buoyant multiplied by the distance for one day (since the mining vessel needs to follow the nodule collector at the seafloor). This initial area is on the order of O(~100 000 m^2). For the 1D model runs we followed the guidelines of WP6: in a “pre”-simulation part the model is relaxated to baseline oceanographic observations for the first 10 years; its end state serves as initial condition for a reference model run and the parameter sensitivity experiments without relaxations.

Experiment \ Parameter	ctl	g1	g2	a1	a2	f1	f2	m1	m2	g1*	g2*	a1*	a2*	f1*	f2*	m1*	m2
K_sed	0.0425									0	0	0	0	0	0	0	0
μ_ZOO	1	0.5	0.0							0.5	0.0						
ε_ZOO	1			0.5	0.0							0.5	0.0				
κ_ZOO	1					0.5	0.0							0.5	0.0		
λ_ZOO	1							1.5	2.0							1.5	2.(

*Table 5.1.1: Overview of the parameter settings of the model sensitivity experiments. ctl = "standard" set of the parameters (which are kept unaltered in the other experiments if not stated otherwise). The experiment labels denote the different processes: g = grazing, a = assimilation, f = fish / higher-trophic fauna, m = mortality), where the respective parameter is changed. For comparison, this set of experiments was run with and without the effect of reduced light attenuation (the latter indicated by the * symbol: ksed=0).*

Exemplarily we present here model results for sediment injection at 65 m water depth for 4 weeks (Fig. 5.1.1). The preliminary results indicate that phytoplankton concentration (A.) gets reduced as well as its growth rate (not shown), which is mainly due to the increased light attenuation, and thus, light limitation. This leads to a reduction of primary production of around 22% for the simulated period of May to August and a reduction in export production of around 28% as well as a decline in the oxygen production (E.), while concentrations of nutrients, such as phosphate (H.), increase. Zooplankton concentrations (B.) decline due to reduced grazing, and decreased detritus production (C.) follows phytoplankton and zooplankton patterns with the effect of decreasing dissolved organic phosphorus concentrations (G.) as well as its remineralization (not shown).

The results of the different model experiments for a sediment injection depth at 65 m and different discharge times are compared in Figure 5.1.2. The boxplot indicates that increased light attenuation gives the largest effect for the sediment injection in the euphotic zone at 65 m. The direction and magnitude of changes in all experiments in A. to D. are comparable for each discharge time with patterns similar to the example experiment (65m_4w, Fig. 3.2.1). However, when excluding the light attenuation effect, different parameters appear to lead to different effects. A reduced maximum grazing rate (μ_{zoo}=0.5) leads to an increase in phytoplankton with some shift to increased detritus. Mainly zooplankton is reduced when reducing the assimilation rate (ϵ_{zoo}=0.5) and therefore detritus increases, while a reduced density dependent loss rate (κ_{zoo}=0.5) increases mostly zooplankton with the

effect of reduced detritus. We can, however, also point out that extreme cases (μ_{zoo}=0.0, ϵ_{zoo}=0.0 and κ_{zoo}=0.0) lead to similarly strong impacts as light limitation, in particularly on zooplankton with strong decreases in the first two and increase in the last case. For longer sediment injection times of 26 weeks and the extreme cases of μ_{zoo}=0.0 and ϵ_{zoo}=0.0 we can also find strong increases in detritus as clearly zooplankton is not able to graze or assimilate on phytoplankton to be turning directly to detritus and therefore being exported to depth.

Figure 5.1.1: Preliminary results for the experiment 65m_4w (discharge of 1.2 kg/s for 4 weeks at 65 m water depth) with sediment concentration [g/l] due to injection on the left-hand side of each panel (brown color bar). This experiment includes the effect of increased light attenuation due to the injected sediment concentration. Each panel (A. – H.) shows the absolute difference for each stated variable in the respective units. Dashed and solid contour lines represent negative and positive values. For comparison the side-panels of A. – H. illustrate the mean profile of the unimpacted reference-simulation for the same period.

Figure 5.1.2: Boxplots showing relative differences [%] between experiments and reference for each variable (A. – H.) taken from the depths amidst 50m and 150m for twice the discharge periods from injection start. Each group of boxplots (color-coded) follow the order of discharge times: 1/4/8/26 weeks. In white boxplots the ctl-experiments are shown without changes in the impact parameter in presence of light attenuation (included in the first row). The colors in the boxes represent the alterations of parameters to be activated in presence of sediment concentration, which is repeated in the second row without the effect of light attenuation.

Benthic biogeochemical simulations of dissolved oxygen concentrations in the mined areas show that after the removal of the top seafloor sediment layer (on average about 5 cm; Gazis et al., 2025) and redeposition of 2-3 cm of suspended plume material, oxygen is freely diffusing into the sediment and oxygen consumption by microbial organic matter degradation is essentially zero (Fig. 5.1.3). This can be explained by the removal of almost the entire bioturbated layer (5-7 cm in the Clarion-Clipperton Zone; Volz et al., 2020), including its endofauna, which is the most reactive microbial layer of the sediment. Our benthic simulations predict that it takes thousands of years for the process to recover (Haffert et al., 2020; Volz et al., 2020).

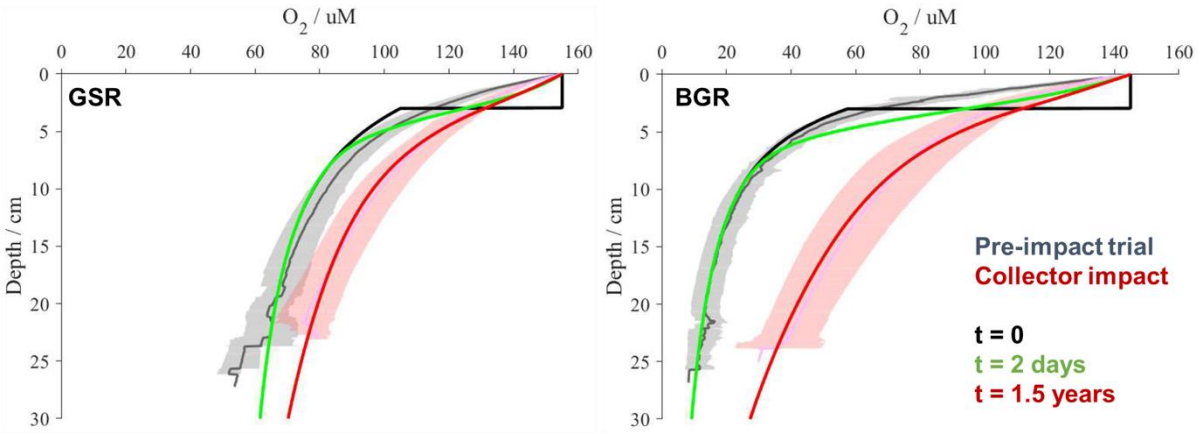

Figure 5.1.3: Simulated dissolved oxygen concentrations (solid lines) compared to in situ measured microprofiles (shaded areas indicating mean and standard deviation of the pre-impact situation (gray) and 1.5 years after the mining (red)). Model results are shown for the start condition (t=0; after removal of 5 cm and redeposition of 3 cm fully oxygenated plume material layer), after 2 days (green) and after 1.5 years (red). Simulations were carried out for the GSR (left) and BGR (right) contract areas in the Clarion-Clipperton Zone of the NE equatorial Pacific.

Description of data set

The preliminary pelagic model dataset contains phytoplankton, zooplankton, and detritus concentrations (in mmol P / m^3), dissolved inorganic carbon and nitrogen concentrations, dissolved oxygen concentration as well as dissolved organic phosphorus and phosphate concentrations for the described model scenarios and parameter variations (Tab. 5.1.1). The relevant carbon metrics are currently extracted from the model results (primary production, carbon fluxes and inventories). Location: 10.5281/zenodo.16912180

Since the recovery of benthic biogeochemical processes takes thousands of years, but the intended DST model run times are only years to maybe a couple of decades, it is sufficient to simply set the benthic carbon remineralization rate to zero as well as associated nutrient fluxes from the sediment into the water column.

Task 5.2: Impacts of sediment generating (e.g. dredging, trawling) activities on the shelf sea ecosystems

The North Sea Benthos Survey (NSBS; Heip et al. 1992), covering the entire North Sea, represents one of the most comprehensive benthic data sets in terms of shelf coverage. In spite of its old age (1986), the data provide valuable information regarding human impacts on the marine ecosystem at a stage where some pressures on the sea floor were declining while some others were rising.

We assessed macrozoobenthic carbon dynamics under the effect of bottom trawling that has been practiced for decades in the North Sea (Callaway et al. 2007, Kerby et al. 2012). Recently, the extent of the main bottom trawling activities was reconstructed over thirty years from the 1980's (Couce et al. 2020), which enables the quantification of biomass variations before and after trawling disturbance. NSBS data provide individual organism densities at 234 sampling stations (Fig. 1a). As biomass is crucial for quantifying carbon content, we used median ash free dry mass per species, documented from the literature, after what we multiplied those values by individual densities in order to get biomass densities per square meter. As the carbon fraction in benthic ash free dry mass is relatively constant among taxonomic groups (circa 50 %; Salonen et al. 1976, Clarke 2008), we divided biomass densities by two to obtain estimations of macrozoobenthic carbon density.

In a recent work, Beauchard and Soetaert (under review) proposed a modelling procedure to back calculate benthic faunal abundance preceding bottom trawling disturbance (carrying capacity). Inspired from a previous development (Pitcher et al. 2016) and based on the logistic population growth, the procedure returns the "relative benthic status" as the ratio between observation (possibly impacted) and carrying capacity (reference). Two biological traits are used to model organism response to trawling gear. Instantaneously, burying depth characterizes organism's exposition to the gear and consequent mortality rate, while age at maturity is used to approximate the intrinsic rate of natural increase, expressing population recovery rate following disturbance. Out of 552 taxa, 304 were documented for those traits, representing 85 % of total individual density.

Couce et al. (2020) provided a reconstruction of beam and otter trawling efforts (hours per year) in the North Sea from 1985 to 2015. We used the quite stable series between 1985 and 1990 to approximate the average trawling disturbance frequency around the sampling period. As NSBS stations are located at the intersections of the ICES rectangles of the shapefile, we simply interpolated the fishing effort before extracting the values corresponding to the sampling locations. Then, we used the trawling gear penetration depth values provided in Pitcher et al. (2022), with adjustment for otter trawl according to van der Reijden et al. (2025).

Model outputs are displayed in Figure 5.2.1.

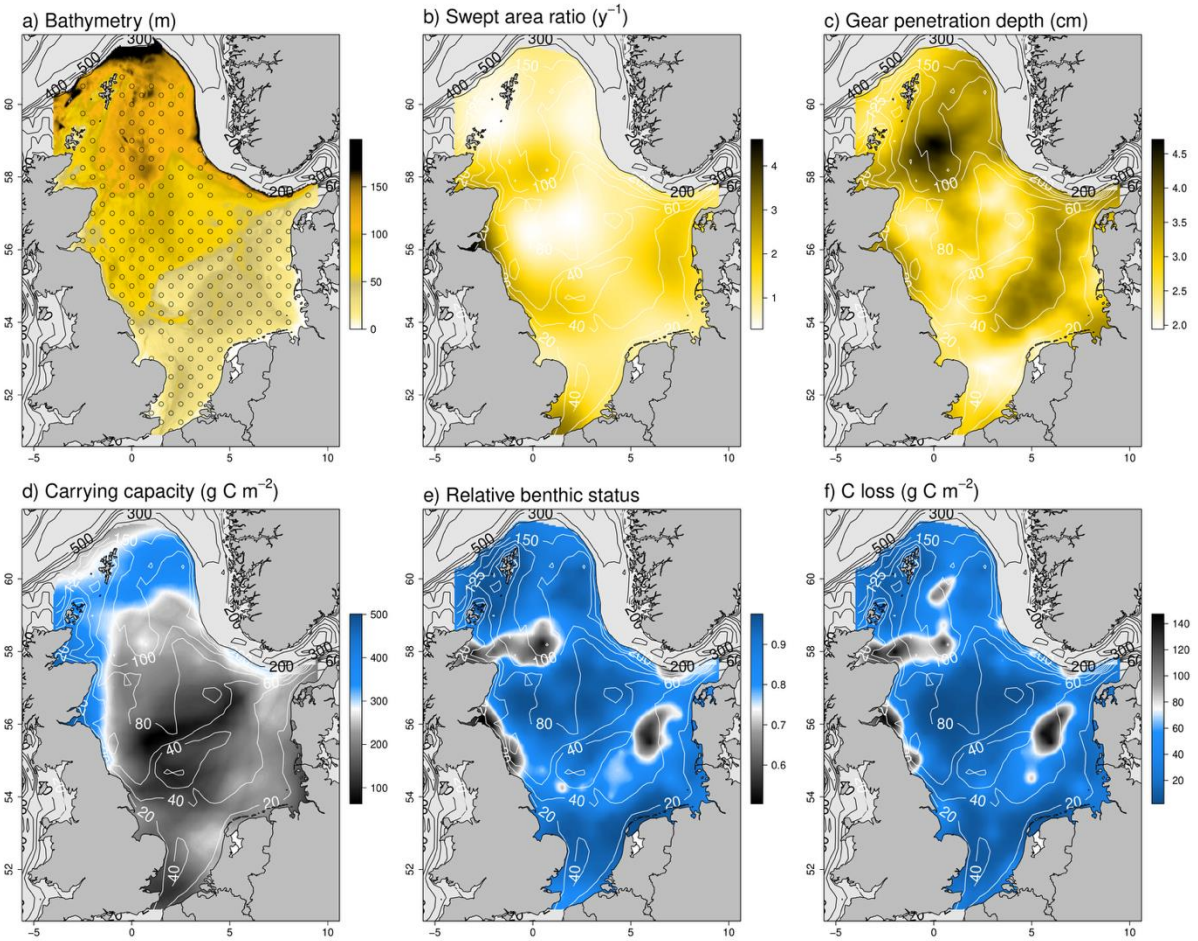

Figure 5.2.1: Carbon dynamics in the North Sea benthos under the effect of bottom trawling. a) Bathymetry; dots, sampling locations. b) Trawling intensity as the number of times the location is trawled per year. c) penetration of the trawling gear into the sediment; in general, deeper in mud than in sand. d) Macrozoobenthic carbon carrying capacity, modelled before bottom trawling impact. e) Relative benthic status as the ratio between observed macrozoobenthic carbon density to carbon carrying capacity. f) Density of carbon lost following bottom trawling disturbance (i.e., carrying capacity minus observation).

Description of data set

Two objects are provided: a sampling stations x variables data frame (csv file) and a raster brick of smoothed values (grd and gri files):

- longitude, latitude: geographic coordinates of the sampling stations (WGS84)
- depth: water depth in m
- sediment type: qualitative variable, 5 categories from very muddy to very sandy
- swept area ratio: bottom trawling frequency as the number of times an area in trawled (per year)
- gear penetration depth: averaged penetration of the bottom trawling gear into the sediment in cm

- observed C content: organism carbon content (g C m2) as ash free dry mass (g m2) devided by 2
- C carrying capacity: organism carbon content back-calculated prior to trawling disturbance
- relative benthic status: ratio of observed organism carbon content by back-calculated content
- C loss: back-calculated organism carbon content minus observed content

Location: 10.5281/zenodo.16794849

Task 5.3: Impacts of fishing on carbon sequestration in shelf ecosystem

Irish Sea EwE

The **Irish Sea EwE** is a peer-reviewed food web model of the Irish Sea developed by Bentley et al. (2019). The Irish Sea EwE model was designed to investigate the dynamics of commercially important species, and the fish component is well-defined. We used the Irish Sea EwE model and past data (1973- 2016) to run two fishing scenarios and used the outputs of Ecosim with offline equations to estimate fish C flux to the seafloor in a continental shelf region. The results quantify carbon flux from the fish community in fish faecal pellets and carcasses. The attenuation of faecal pellets in the water column is accounted for in the calculations.

Two scenarios were assessed. Firstly, the reported fishing scenario, as used in the Irish Sea EwE key run, models past fishing practices as reported, informed by data from fishing records. Over the modelled time (1973- 2016), the average fish C flux to the seafloor was 3.95 mgC $m^{-2}d^{-1}$. Secondly, we maintained all the same Irish Sea EwE key run settings, but did not include any fishing in the simulation. Over the modelled time, the average fish C flux to the seafloor was 3.78 mgC $m^{-2}d^{-1}$. Simulation results showed an increase in the biomass of the fish community; however, they did not show a big difference in fish C flux to the seafloor.

The results showed that increasing biomass by stopping fishing did not result in an increase in fish C flux to the sea floor. The relationship between fishing management and fish C flux is complex, as changes in the composition of fish functional groups (i.e., increased biomass of some species led to changes in biomass proportions within the functional group) and differences in biological

parameters related to the fish species, such as the consumption-to-biomass ratio and natural mortality.

Description of data set

The data includes carbon fluxes from EwE model runs. These estimates come from outputs of Ecosim runs linked to offline equations to estimate carbon fluxes by the fish comunity. Irish Sea carbon flux is measured in mgC $m^{-2}d^{-1}$. The simulations of the Irish Sea EwE model run from 1973 to 2016.

Data is available in .csv format and contains the following variables:

- *Year*
- *Cflux*: Total fish-mediated carbon flux to the seafloor in the reported fishing scenario
- *Cflux_nofishing*: Total fish-mediated carbon flux to the seafloor in the no-fishing scenario

The data set is published in Zenodo with DOI:10.5281/zenodo.16539668.

StrathE2E Celtic Sea

StrathE2E is an end-to-end ecosystem model, describing the entire food web within shelf regions, from inorganic nutrients to megafauna, including bacterial degradation (Heath et al., 2021). The model is combined to a fishing fleet model which simulates seabed disturbance caused by different fishing gears. As all outputs from StrathE2E are nitrogen fluxes, a post-processing algorithm is being developed to convert them accurately into carbon fluxes. Results from the first version of this algorithm is presented in this section.

Methods

A simple approach for converting StrathE2E nitrogen fluxes into carbon would be to use the Redfield atomic ratio of carbon and nitrogen (C_{106}:N_{16}). This ratio describes carbon-nitrogen stoichiometry in plankton assumed to be globally constant (Redfield, 1934, 1958; Redfield et al, 1963). However, compiled data from literature and open-access datasets showed that C:N ratios tend to decrease when trophic level increased (Figure 5.3.1). Other studies have observed a similar relationship between carbon-nutrient stoichiometry and trophic level in marine environments (Sterner and Elser, 2002; Scharler et al., 2015; Guo et al., 2022).

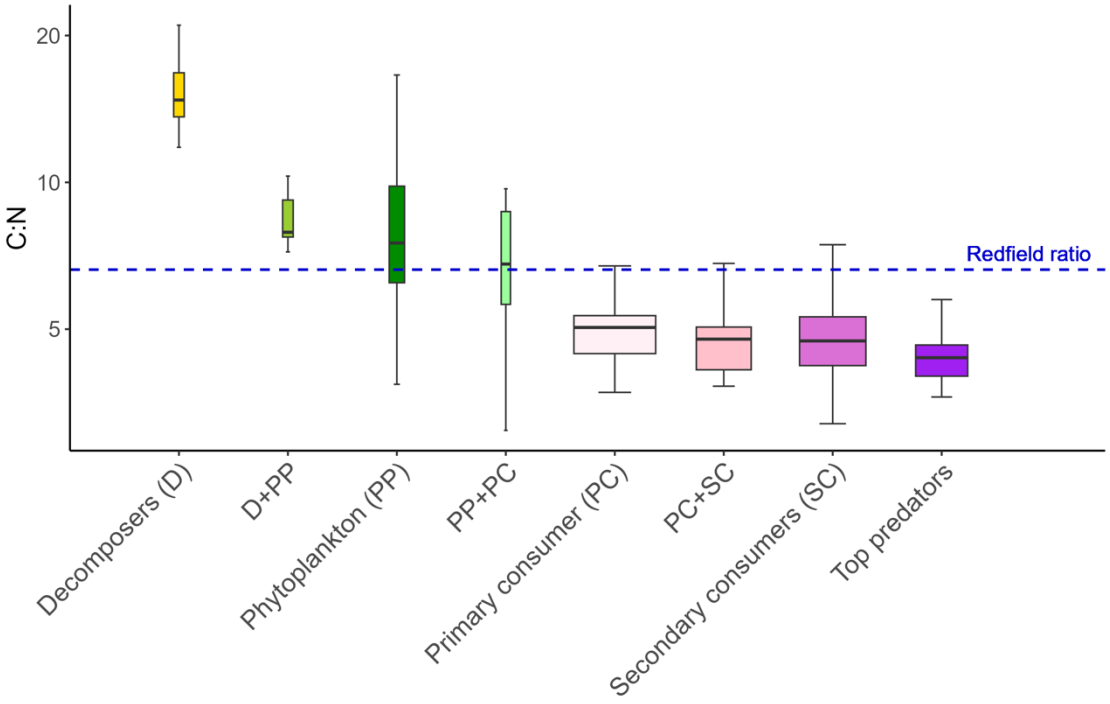

Figure 5.3.1. Distribution of carbon-nitrogen (C:N) ratio per trophic group observed in compiled data set of carbon-nitrogen stoichiometry. Box widths are scaled to the quantity of data compiled for their trophic group. (Data sources: Vanni et al, 2017; Schiettekatte et al., 2020; Guo et al., 2022; Koch and McCarthy, 2016; Acevedo-Gutierrez et al., 2012; Rynearson, 2019)

Carbon-nitrogen stoichiometry in consumers is assumed to be affected by the stoichiometry of their ingested food and their ability to assimilate the different elements. Based on previous observations, the initial assumption was that consumers are unable to assimilate a certain fraction **q** of carbon from their diet which is dumped directly to faeces and would explain C:N ratio decrease with increasing trophic level. This parameter **q** was also assumed to be constant for all consumers. In StrathE2E outputs, nitrogen uptake, assimilation and excretion fluxes by consumers can be derived from the model's differential equations (Heath et al., 2021). Thus, for each consumer, if C:N ratios of all preys are known, it is possible to calculate both the carbon flux from consumer to water-column detritus and the consumer's own C:N ratio, by using the values of nitrogen uptake and parameter **q**. Other nitrogen fluxes can then be converted to carbon by using the flux source's C:N ratio. However, due to the complexity of the food web structure, the conversion algorithm must compute carbon fluxes iteratively following these four steps:

Step 1 - Initialize C:N ratio of every guild to the Redfield ratio, except for macrophytes (kelp). In StrathE2E, macrophytes are the only guild with carbon outputs (Heath & Speirs, 2023), and their C:N ratio can be computed directly from these outputs.
Step 2 - Using the current values of C:N and nitrogen outputs, calculate all carbon fluxes.
Step 3 - Except for macrophytes and phytoplankton, update C:N ratio of each guild. Phytoplankton stoichiometry is assumed to follow the Redfield ratio.
Step 4 - Repeat step 2 and 3 until full convergence.

Parameter **q** was optimised for StrathE2E baseline models (see below) so that C:N ratios obtained from the N-to-C conversion algorithm would be the best fit to C:N ratios from compiled observations (Vanni et al, 2017; Schiettekatte et al., 2020; Guo et al., 2022; Koch and McCarthy, 2016; Acevedo-Gutierrez et al., 2012; Serpetti, 2012). C:N ratios were log-transformed before the mean squared error (MSE) was calculated as measurement of fitting success. Selected parameter value resulted in an MSE of 0.066.

The Celtic Sea implementation was chosen for the first application of the N-to-C conversion algorithm. This covered the shelf regions South-West of Ireland and England with seabed habitats mostly defined by sandy sediment (Figure 5.3.2). The model was fitted over the period 2010-2015 on historical fishery data, with inputs from the NEMO-ERSEM coupled hydrogeochemical model runs which has historical hindcast until 2015 (Artioli et al., 2023). Four different runs of NEMO-ERSEM were used as inputs and resulted in different variants of the Celtic Sea model. These four runs were defined by their atmospheric forcing coming from two different CMIP6 models (CNRM or GFDL) and by the climate scenario considered for future projection (SSP1-2.6 and SSP3-7.0). Fitting of parameter **q** was therefore repeated for each atmospheric forcing (CNRM and GFDL). Baseline models with historical fishing were run from 2010 to 2019. Other decades are also available for projection runs until 2069 (outputs from 2040-2049 are available in the StrathE2E data set).

For each Celtic Sea model variant (CNRM or GFDL, SSP3-7.0 or SSP1-2.6, 2010-2019 or 2040-2049), the two following scenarios were tested: (1) historical fishing, and (2) no fishing at all. For the second scenario, it is important to note that any seabed disturbance caused by fishing activities was also removed from the simulation. For each run, carbon fluxes were calculated using the N-to-C conversion algorithm for the whole model domain (inshore and offshore zones combined).

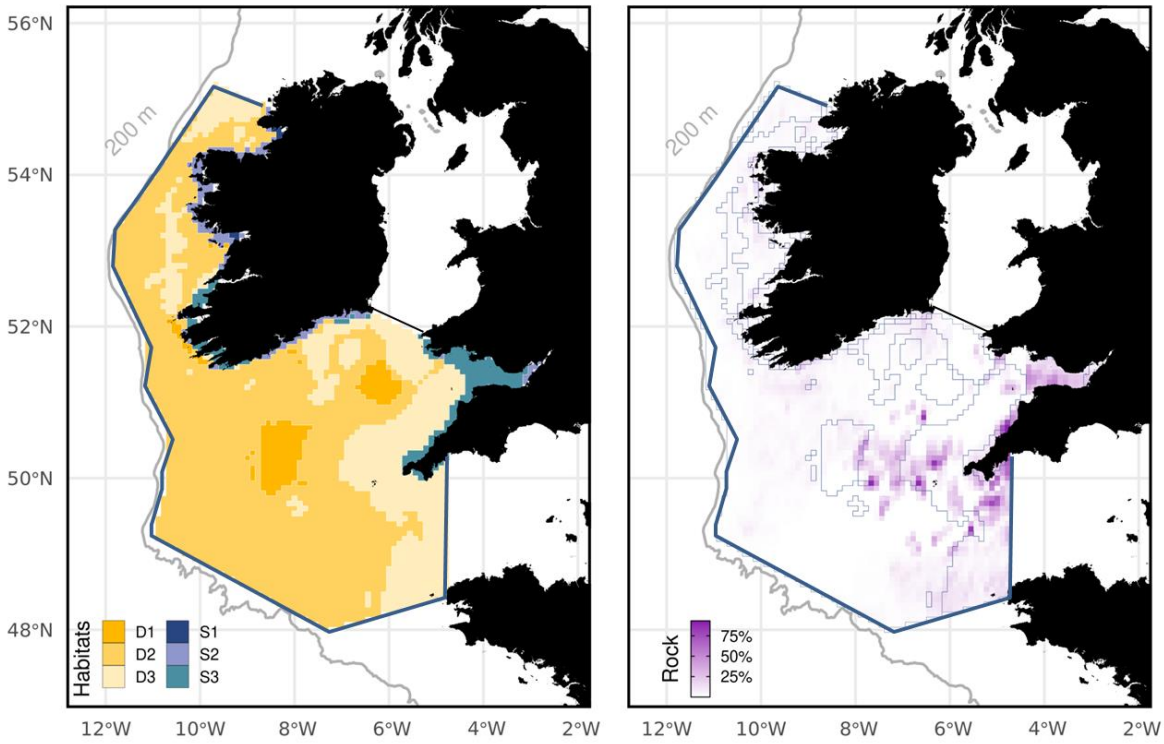

Figure 5.3.2. Celtic Sea model domain and seabed habitats. The model domain is divided into inshore (habitats noted S in left legend, shallower than 30 m) and offshore (D habitats). Seabed habitats (left panel) are defined by grain size with the following classes: (1) fine (muddy, ~0.1 mm), (2) medium (sandy, ~0.3 mm) and (3) coarse (gravel, >1 mm). Within each of the sediment habitats a proportion of the seabed area may present as exposed bedrock (right panel) which has different geochemical properties and in the inshore zone supports the kelp forests which are included in the model food web. Sedimentary data are from Wilson et al. (2018).

Simulation results

For all model variants tested here, a light decrease in carbon net burial (<1%) was observed when removing all fishing activities. For example, in the CNRM-SSP3-7.0 model simulation over 2010-2019, annual carbon sequestration was 20.7 g C. $m^{-2}.y^{-1}$ with fishing and 20.6 g C. $m^{-2}.y^{-1}$ without fishing (Figure 5.3.3). This light decrease went along with a light increase in both CO_2 release and faecal pellets (both <1%), suggesting a small increase in consumer activity and biomass.

In the Celtic Sea, kelp harvesting is a sizeable activity in fishery. In average from all simulations with fishing, 65.1% of the carbon extracted by fishery was due to kelp harvesting activities (Figure 5.3.4). In contrast, fish and benthos represented only 32.2 and 2.3% of the annual landings in carbon.

Seabed living animals seem to play an essential role in carbon sequestration in the Celtic Sea. Indeed, among consumer guilds, benthos produced the most corpses (99.4%) and were second most faeces producers (40.3%) behind zooplankton (58.7%). In comparison, fish contributed 0.9% of faeces

production and 0.6% of corpses production, while whales contributed 0.03% of faeces and <0.01% of corpses. In addition, 95.3% of faeces produced by benthos were directly transferred to sediment, the rest joining the water column detritus pool. Benthos faeces represented 64.4% of the total organic carbon inflow to sediment, while the rest came from sinking corpses (30.9%), kelp debris (4.6%) and water column detritus (0.01%, *inc.* faecal matter in water column). In StrathE2E, carbon burial flux to seabed comes solely from refractory detritus in sediment. In the Celtic Sea, refractory sediment detritus had inflows from labile sediment detritus (64.3%, of which 77.5% came from benthos), corpses (27.4%) and kelp debris (8.3%). According to all these fluxes, benthos could be responsible for up to 77% of the organic carbon sequestrated in the seabed of the Celtic Sea (faeces and corpses fluxes combined).
Compared to the StrathE2E carbon sequestration estimates obtained with the N-to-C conversion algorithm, a simple conversion using the Redfield ratio for all fluxes would underestimate carbon sequestration by about 4% on average. In the case of the CNRM-SSP3-7.0 Celtic Sea simulation in 2010-2019, annual carbon sequestration would have been estimated at 19.9 g C. $m^{-2}.y^{-1}$.

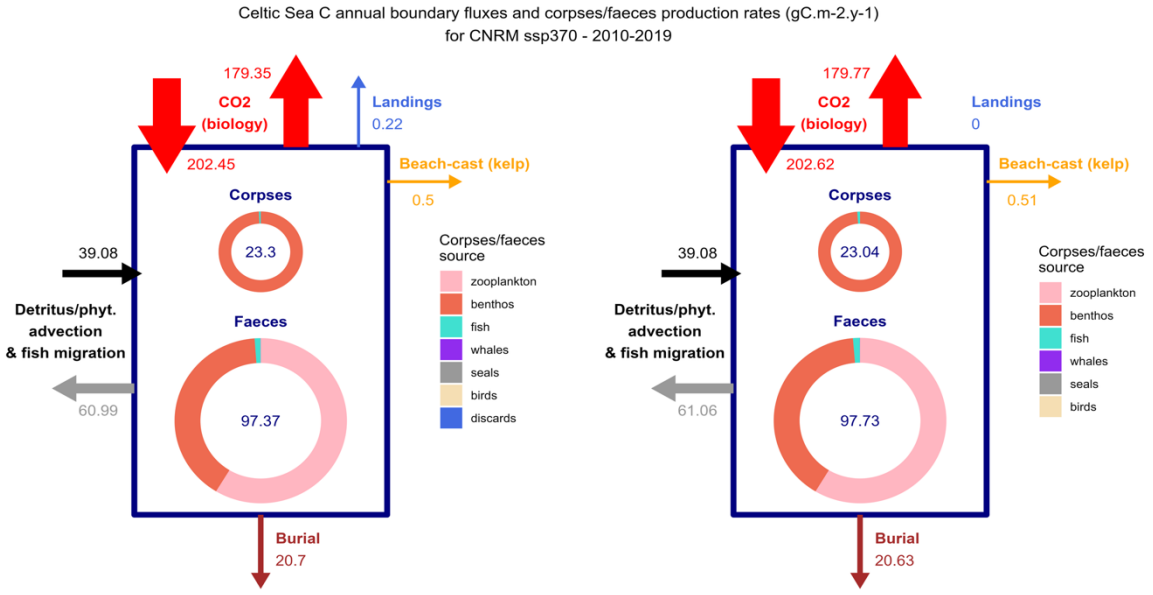

Figure 5.3.3. Annual boundary fluxes and annual corpses/faeces production rates (g C.$m^{-2}.y^{-1}$) in the Celtic Sea from StrathE2E model runs for 2010-2019, either with historical fishing (left diagram) or with no fishing effort (right diagram). The blue box represents the food web for the whole model domain (combining both inshore and offshore zones) and arrows represent flows of carbon in or our the food web. Inside the box, annual production rates of corpses and faeces (also fluxes but within model boundaries) are given with contributions from the different guilds. Note that (1) zooplankton guilds do not contribute to the flux to corpses when they die in StrathE2E, due to their small sizes, (2) a discard flux is present and contributes to the flux to corpses only when there is fishing activity, (3) the value for inflow of detritus/phytoplankton and fish into the system (black arrow) comes directly from input data,

and (4) there is no dissolved inorganic carbon (DIC) inflow or outflow represented here, which is why the system seems out of balance (boundary fluxes do not sum to zero).

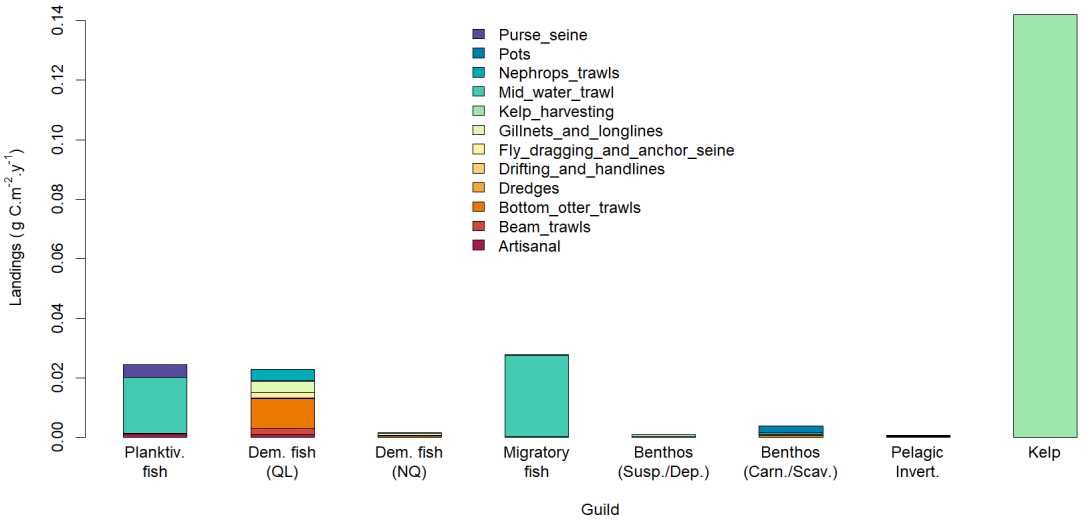

Figure 5.3.4. Annual fluxes of carbon extracted by fishery activities (g C.m^{-2}.y^{-1}) in the Celtic sea per guild and fishing gear.

Description of data set

Dataset includes carbon fluxes computed by postprocessing nitrogen outputs from StrathE2E model runs, by taking into account carbon-nitrogen stoichiometry dynamics in the food web. For each model variant, the following data are available in csv format:

- Carbon budget data ("#_Cbudget-data.csv")
- Matrices of annual carbon and nitrogen fluxes for whole area (inshore and offshore zones combined) from last year model outputs ("#_C-fluxes.csv" and "#_N-fluxes.csv")
- Landings by guild (e.g. planktivorous fish, pelagic invertebrates, benthos, birds...) and by gear (e.g. beam trawls, dredges...) in carbon and nitrogen units ("#_C-land-by-gear.csv" and "#_N-land-by-gear.csv")

In addition, the "CN-ratios_all-model-variants.csv" file compiles all resulting C:N ratios of each guild for each model variant.

Carbon budget data contain summaries of the following boundary and internal (production) fluxes:

- Carbon sequestration (net sediment burial)
- Landings

- Discards
- Corpses (note that discards end up in this guild after a short lifetime (see flux matrices))
- Faecal pellets
- CO2 absorption by food web guilds
- CO2 release by food web guilds
- Beach cast of macrophytes (kelp)
- Passive inflow of organic carbon (from phytoplankton and detritus) from open ocean
- Passive outflow of organic carbon (from phytoplankton and detritus) from open ocean
- Fish migration inflow
- Fish migration outflow

For each variable, both the total annual flux and flux by guild are given.

In carbon and nitrogen flux matrices, each column represents the destination/consumer guild and each row the source/prey guild.

> Example: the value read in row "carnzoo" (carnivorous zooplankton) and column "pfish" (planktivorous fish) is the annual flux of consumption of carnivorous zooplankton by planktivorous fish.

These matrices also include boundary fluxes (e.g. open ocean, atmosphere...). All fluxes are given in $mmol.m^{-2}.y^{-1}$ of either carbon or nitrogen.

The dataset is published on Zenodo (StrathE2E dataset) with DOI:10.5281/zenodo.16601930.

EwE in the Celtic Sea

This Ecopath model is an extension of the Potier et al., (2024) model and is the last update of multiple models Guénette et al., 2009 ; Moullec et al., 2017 ; Hernvann et al., 2020). It is aimed at exploring the effects of fish removal on carbon dynamics. We study carbon pools (living, labile detritus, refractory detritus) and flux between them and the environment (e.g. CO_2 exchanges). Here, we will focus on the flux of particulate organic carbon (POC), with an emphasis on POC production by fish.

Methods

We simulated ecosystem dynamics from 2003 to 2050 with Ecosim, with the first 2003-2020 years being fitted on data (Potier et al., 2024) and 2021-2050 being the forecasting period. The last year of the simulation (2050) will then

be extracted as an Ecopath model, which is a snapshot of the ecosystem state. From this snapshot, we extract the ecological pools and fluxes.
The forecasting period is split in two scenarios: one with constant current (2020) fishing effort, the other with no fish removal. The Ecopath snapshots of the two scenarios are then compared.

Carbon pools and fluxes were aggregated according to their carbon "state" (living, dead labile and dead refractory) and transitions between these states. In Ecopath, respiration is an export to the environment, so there is no related compartment like atmospheric CO_2. According to the needs, the living compartment may be split in primary producers, detritivores and other consumers. Also, both labile and refractory detritus can be split in their pelagic (sinking or dissolved) and sedimentary fractions.

To compare the scenarios, we adopted a trophic framework (inspired by EcoTroph, Gascuel et al 2011), in which specific groups are abstracted away to keep only their trophic level. The result is a distribution of ecological fluxes (e.g. production, consumption or respiration) over trophic levels, called trophic spectrum. Some of these fluxes can be partitioned in distinct fluxes, such as their biological function such as detritus production being composed of two components, natural mortality and unassimilated food.

The relative change dX associated to the cessation of fishing (in %) of a variable X for a given trophic class was defined as follows:

$$dX = (\Sigma (X_{nf} - X_f) / \Sigma (X_f)) \times 100$$

With X_{nf} and X_f the values of X in the “no fishing” and “fishing” scenario, respectively. Note that this implies that we take the fishing scenario as the reference state of the system.

To disentangle the underlying sources of observed changes, we partitioned some fluxes (e.g. detritus production) according to their components (e.g. natural mortality and unassimilated food). We expected such a partitioning to reveal the dominant biological drivers of detritic production and carbon sequestration.

Results

Fish removal had negligible effect on all major ecosystem fluxes (Fig. 5.3.5). Therefore, the impact of fishing must be limited to exploited groups, fishes in particular. This is exemplified by significant increases in biomass for high trophic levels (Fig. 5.3.6).

It is further confirmed by the change in POC production by fish between the two scenarios (Fig. 3). Cessation of fishing increased fish POC production by

0.14 t/km²/year (+10.3%). This total increase in POC production by fish was heterogeneously distributed across trophic levels (Fig. 5.3.7a). As necroproduction consists of two processes, namely natural mortality and unassimilated consumption (egestion and excretion), we calculated the contribution of each of these processes to the total variation. It appears that unassimilated consumption is the major driver of change in POC production (Fig. 3b).

However, this result should be considered in the larger context of POC production by all organisms, which is only reduced by 1.01 t/km²/year (-0.1%).

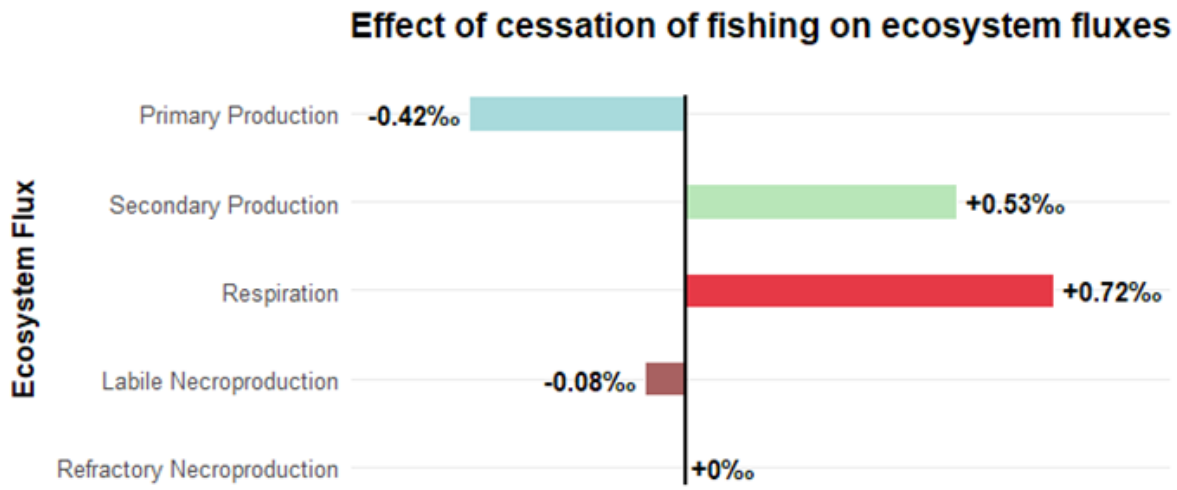

Figure 5.3.5. Effect of cessation of fishing on major ecosystem fluxes. Despite mixed effects of the various fluxes, the impact of fishing on assessed carbon fluxes remains limited (<1‰), or even negligible. Secondary production is production by heterotrophs. Necroproduction is the production of detritus, and includes fluxes between detritic compartments.

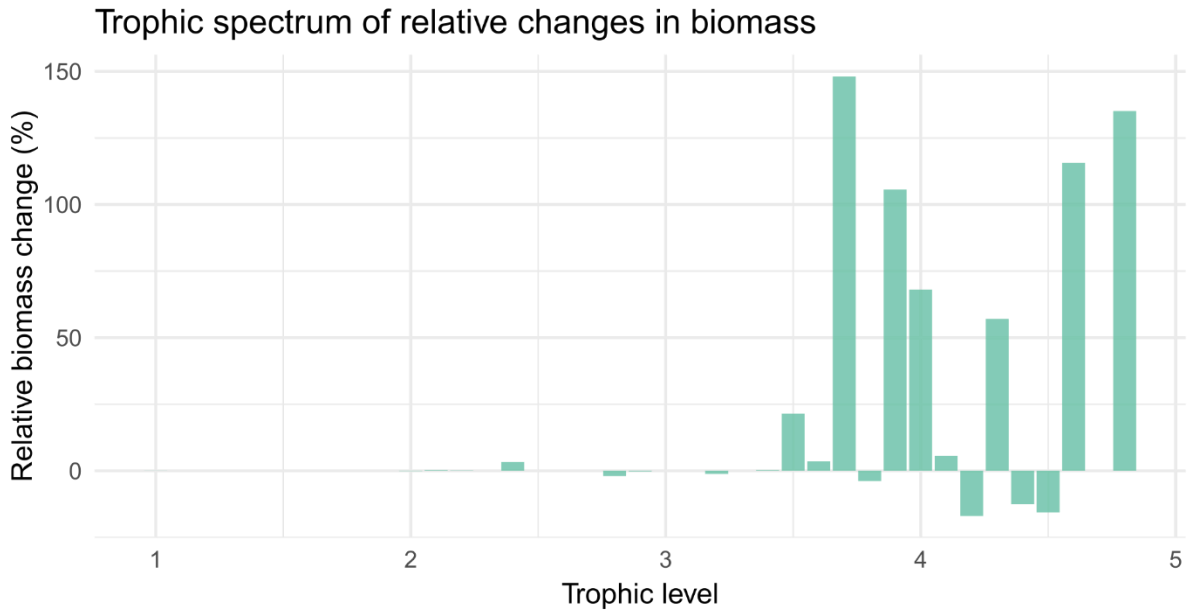

Figure 5.3.6. Relative changes in biomass due to cessation of fishing. Most changes in biomass occur in higher trophic levels and are positive. Although important, these changes are minor in absolute value as most biomass is concentrated in lower trophic levels.

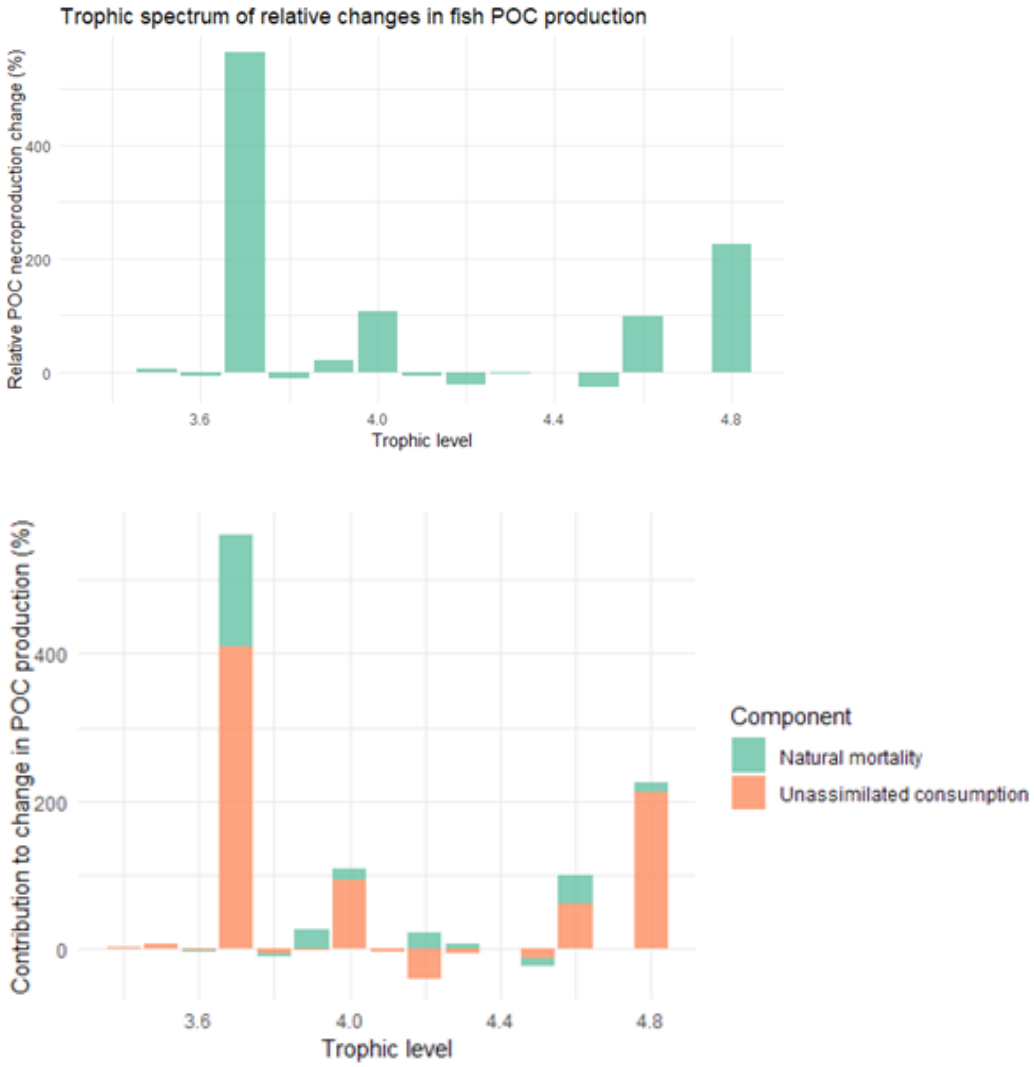

Figure 5.3.7. Relative changes in fish POC production due to cessation of fishing. Note that since we focus on fish, trophic levels are all above 3.5. (A) Response to cessation of fishing in POC production is highly variable across trophic levels, which may highlight complex trophic restructuring. (B) Most of these variations are due to unassimilated consumption, and natural mortality play a minor role in the increase in POC production. Note that in some cases (e.g. TL = 4.2), a change in total POC production may hide opposite changes between the two components. Therefore, an increase in mortality could nonetheless result in a decrease in POC production.

Description of data set

The dataset is published on Zenodo (https://doi.org/10.5281/zenodo.16923795).

Task 5.4: Impacts of fishing on carbon sequestration in off-shelf ecosystems

Simulations with SEAPODYM

To limit climate warming to 2˚C above pre-industrial levels, all economic sectors need to measure their carbon footprint and engage a rapid transformation to reduce as far as possible their carbon emissions. Food production is responsible for a quarter of anthropogenic greenhouse gas (GHG) emissions globally. In many sectors (e.g., agriculture and fisheries), the activity necessarily modifies the natural carbon balance, and these changes need to be estimated in detail to facilitate the reduction of emissions where it is possible, evaluate the cost benefit ratio of the ecosystemic service compared to other existing alternatives, and eventually to estimate what compensation level remains to achieve a net zero emission of CO2.

Oceanic tuna fisheries are a key food production sector that burns fossil fuel to operate (Parker et al 2018) but can also impact the biological carbon pump (BCP) and its carbon sequestration fluxes, by reducing the deadfall of large-bodied fish and the export of fecal pellets sinking in the ocean depths. Part of this sinking carbon matter is remineralized by the microbial loop and reinjected in the surface layer, while the remaining fraction that reaches the deep layers of the ocean can stay for decades to centuries.

The removal of tuna biomass from the ocean has increased over the last decades with the development of the industrial fisheries since the 1970s. In 2023, the total global tuna catch reached 5.2 million tonnes in 2023 (ISSF 2025). It is dominated by skipjack tuna (57%), followed by yellowfin (30%), bigeye (7%), and albacore (5%) tunas. The remainder of the catch is predominately comprised of billfishes, (swordfish and marlins), sailfish, oceanic sharks and bluefin tuna. Two thirds of this global catch come from the Pacific Ocean. Over the last 10 years, the total catch in the entire Pacific Ocean for the four main tuna species has been relatively stable at between 3.2 and 3.5 Mt. The fishing methods are divided into two broad categories. The largest of the two is commonly referred to as the ‘surface fishery’, where purse-seine and pole-and-line vessels target schools of skipjack and the smaller size classes of yellowfin and bigeye tuna in the tropical and subtropical regions. Purse seining accounted for 66% of total catch and pole-and line for 8% (ISSF 2025). The catch from the surface fishery is used for canning but in the case of the artisanal fishery most of the catch goes to the domestic market.

The second category exploits the subsurface of the ocean using longline vessels that target larger bigeye (size > 90 cm Fork Length) and yellowfin (> 70 cm FL) tuna, mostly in equatorial waters for the Japanese sashimi trade and other high-value markets. In subtropical waters (between about 20° and 40° latitude north and south), the longline fishery catches mainly albacore for canning, but also a proportion of high-value yellowfin and bigeye tuna. The longline fishery includes large distant-water freezer longliners targeting either tropical (yellowfin, bigeye tuna) or subtropical (albacore tuna) species and smaller offshore vessels which are usually domestically based, with ice or chill capacity. Longline fishing accounted for 9% of total catches in 2023 but contributes equally to economic income with surface fishing.

Given the complex interactions between the many components of the oceanic ecosystem, the task of estimating the carbon fluxes passing through the main tuna stocks is challenging (Figure 5.4.1). The first key task is to estimate the total biomass of each species tuna population and their dynamics under the combined impacts of fishing, climate variability and now climate change.

Here, using results from the spatial ecosystem and population dynamics model SEAPODYM, we provide an estimate of the carbon footprint for major tuna species, skipkack, yellowfin and bigeye, with contrasted biology and fishing methods, ie surface vs subsurface fishing gears. The estimate is decomposed between the flux of carbon through excretion of unassimilated carbon, that is fecal pellets, the removal of tuna bodies by fisheries compared to the natural sequestration by fish deadfall after natural mortality, and the carbon footprint due to fuel consumption. Before, the first section summarises the method used to estimate the biomass of tropical tuna species with and without fishing, in the Pacific Ocean that is the domain of the study.

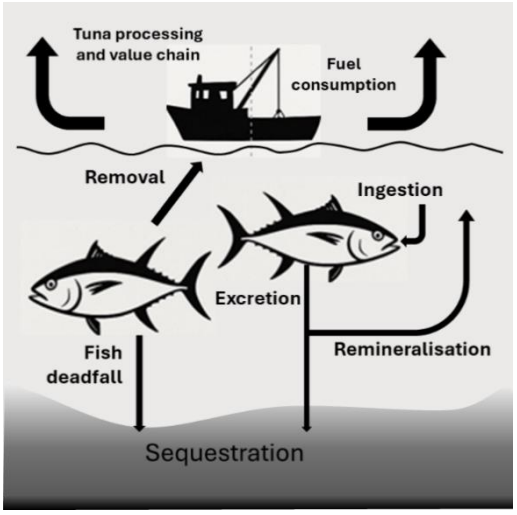

Figure 5.4.1. Schematic view of the processes leading to emission or sequestration of carbon by tuna populations and fisheries in the deep ocean.

Tuna population dynamics under historical fishing and climate variability

The model

Tuna are highly migratory species showing significant basin-scale redistribution in relation to natural climate variability such as the El Nino Southern Oscillation (ENSO). We used tuna catches and simulations from the spatial ecosystem and population dynamics model (SEAPODYM) to assess the spatial distribution of tropical tun species in the Pacific Ocean since the development of the tuna purse seine fishery in the 1980s. SEAPODYM describes the spatial dynamics of tuna under the influence of both fishing and environmental effects, including micronekton biomass distributions that are prey for tuna. The model first simulates the prey dynamics (Lehodey et al. 2010; 2015) and then tuna age-structured population dynamics with different rules changing according to the life stage (Lehodey et al. 2008; Senina et al. 2020; www.seapodym.eu). For example, larvae and juvenile tuna drift with currents but later have autonomous movements (i.e. in addition to the velocities of currents their movements have a component linked to fish size and habitat quality). The predicted distributions of prey, including functional groups of epipelagic and mesopelagic micronekton, drive the movement of tuna feeding on them, considering their accessibility to these prey groups, depending on water temperature and dissolved oxygen concentration. The full explicit modelling of spatial dynamics relies on advection-diffusion-reaction equations (i.e. the density of fish and catch are computed in each cell of a computational grid defined over the model domain). The spatial resolution used was 2˚ x 2˚ and the resolution for time and age dimensions was one month. SEAPODYM also includes a Maximum Likelihood Estimation approach (Senina et al. 2008, 2020) to achieve optimal parametrization taking advantage of the spatially explicit representation by using catch/effort data, and length frequency catch data, available at these resolutions. The fit between observations and predictions is used to validate the optimal solutions of the models.

The reference configuration is driven by temperature, currents, dissolved oxygen, euphotic zone and primary production generated by the coupled model NEMO-PISCES (Nucleus for European Modelling of the Ocean, Pelagic Interaction Scheme for Carbon and Ecosystem Studies). Historical fishing data are provided by SPC and IATTC. This model configuration and its results have been described in detail for the historical fishing period in Senina et al. (2020a; 2020b); Hampton et al. (2022) and Nicol et al. (2022). **The model including micronekton and tuna variables and outputs are archived online**.

Impact of fishing on tuna biomass

Skipjack tuna (*Katsuwonus pelamis*) is a small (30 cm long and 3 kg weight on average) and fast-growing short living species (maximum age of 6+ years), while bigeye tuna (*Thunnus obesus*) reaches much larger sizes (140 cm long and 90 kg weight on average) and is a slow-growing long-living species (maximum age of 12+ years). Yellowfin tuna stands between the two (maximum age of 8+ years).

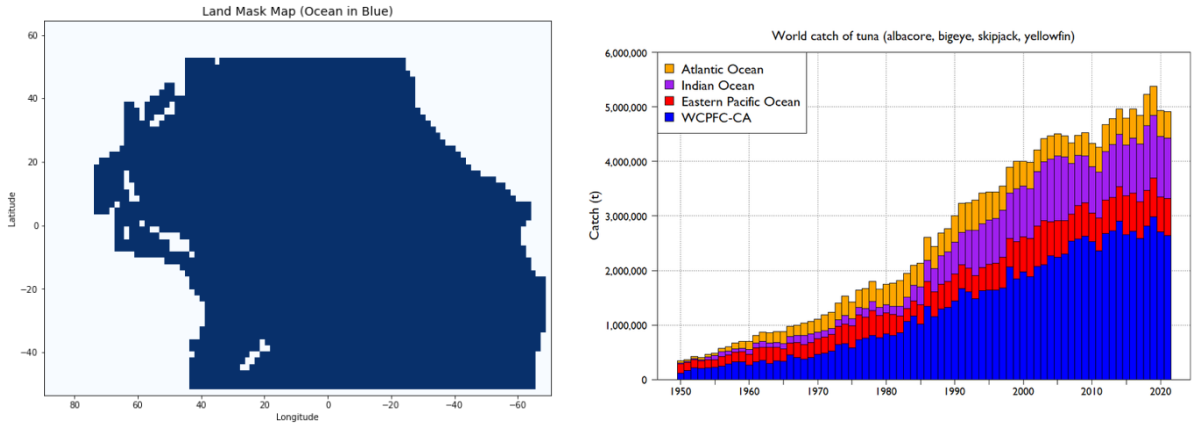

Figure 5.4.2. Left: Model domain for the Pacific Ocean with land mask at resolution of 2 degrees with WCPFC and IATTC RFMOs convention areas; Right: World catch of tuna by Ocean (From Hare et al 2023)

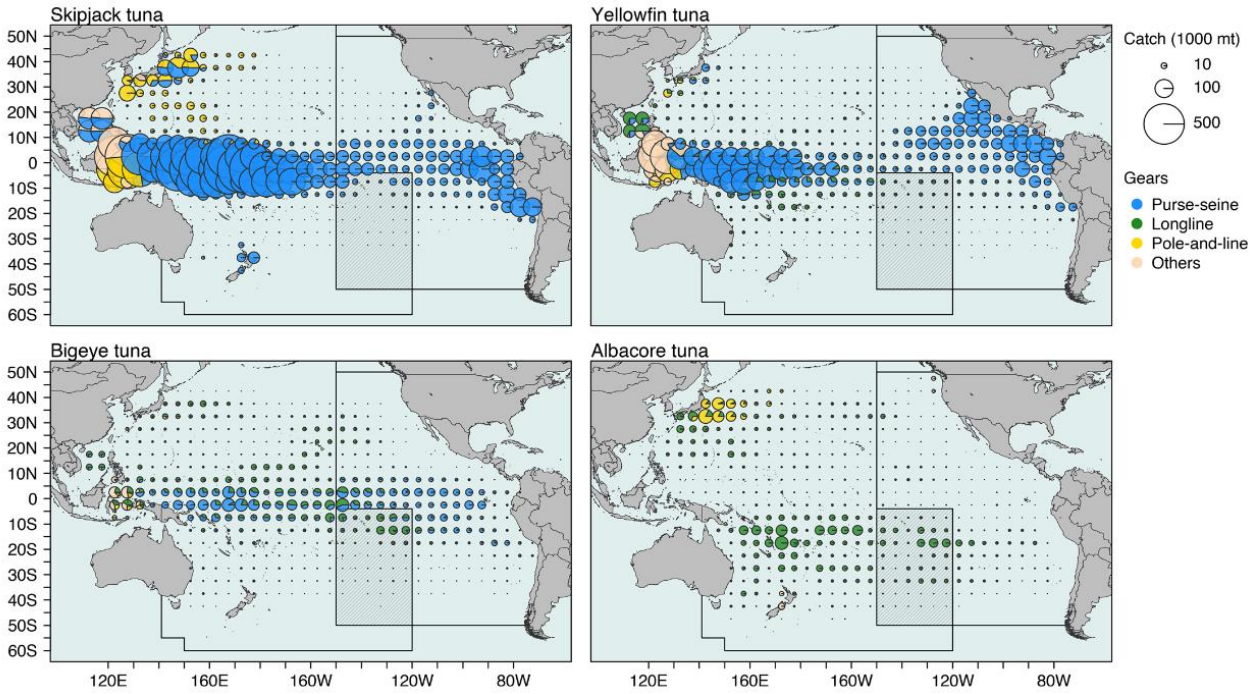

Figure 5.4.3. From Moore et al. (2020). Distribution and magnitude of total catches for skipjack, yellowfin, bigeye and albacore tunas in the Pacific Ocean between 2009–2018 by 5° square and fishing

gear: purse-seine (blue), longline (green), pole-and-line (yellow) and others (pink). The shaded area represents the overlap in management area between the Western and Central Pacific Fisheries Commission (WCPFC; west) and Inter-American Tropical Tuna Commission (IATTC; east) Convention Areas. Note that pies are positioned at the centre of each 5° square and only those catches > 1 mt are shown. Source: Pacific Community (SPC), supplemented by IATTC Public Domain Data (available at: https://www.iattc.org/PublicDomainData/IATTC-Catch-by-species1.htm).

Outputs of the reference simulations that achieve the best score with historical fishing data show a decrease in the Pacific fish stocks from 10.9 Megatonnes (Mt) for the skipjack tuna in 1983 to 9.5 Mt in 2009 and from 4.2 Mt for the bigeye tuna in 1983 to 2.8 Mt in 2009 (Figure 5.4.3). This decrease is mainly associated with the increase in exploitation rate (% of the total biomass removed by month) from 0.5% for the skipjack tuna in the 1980s to 1.5% in 2009 and from 0.33% for the bigeye tuna in the 1980s to 0.62% in 2009 (Figure 5.4.3). By contrast, a scenario without fishing over the same period shows a fluctuating but stable skipjack tuna stock and a slight increase in the bigeye tuna stock (Figure 5.4.4).

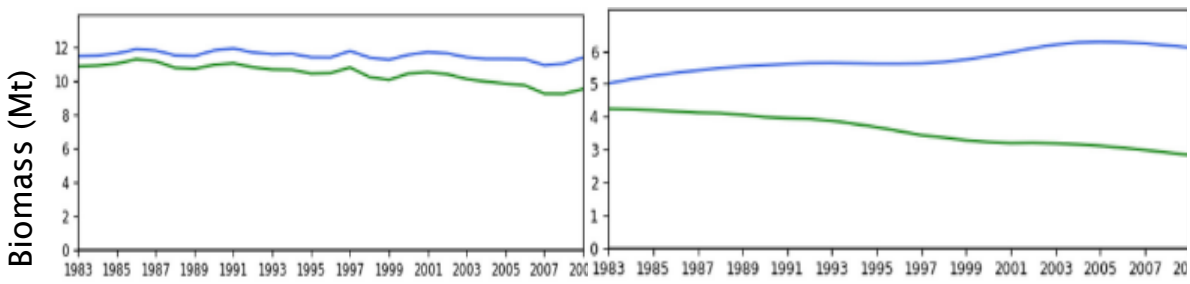

Figure 5.4.4. Temporal trends of biomass since 1980 estimated in the Pacific Ocean for skipjack (Katsuwonus pelamis, left panels) and bigeye (Thunnus obesus, right panels).

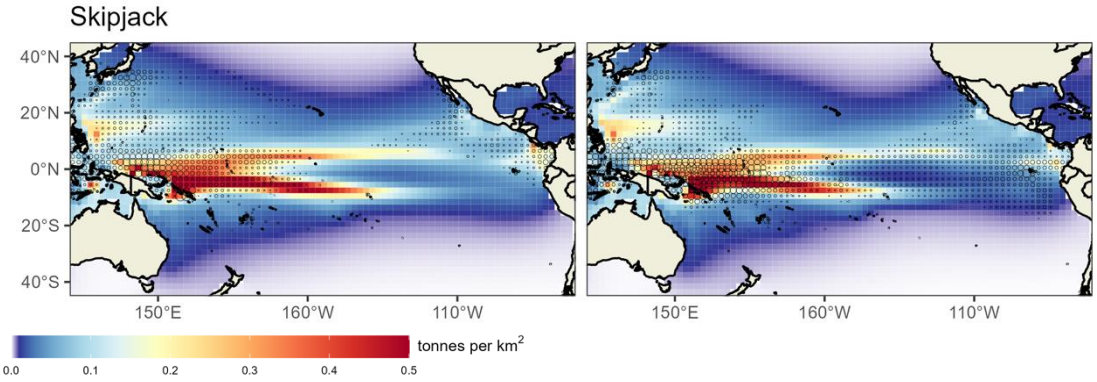

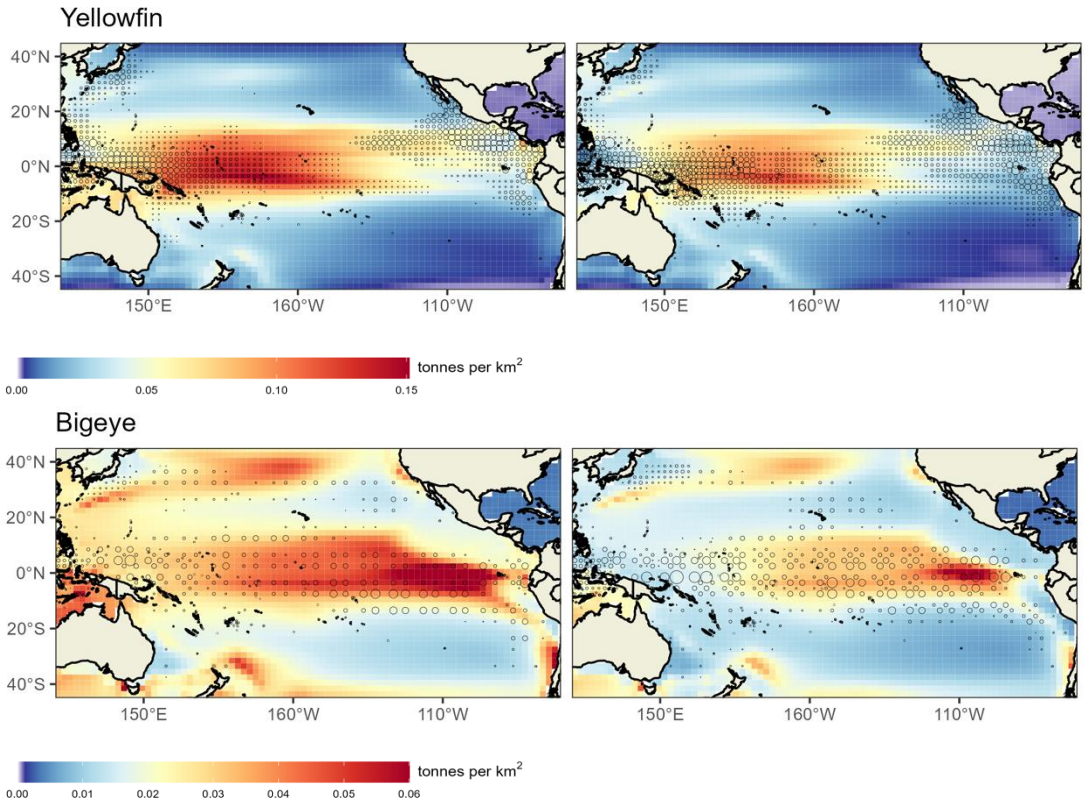

Figure 5.4.5. Comparison of predicted distributions of tuna total biomass (t km^{-2}) using SEAPODYM for 1st and last decade of the historical time series. Total observed catches are shown, with catch proportional to the size of the circles (same scales between decades). Redrawn from Lehodey et al. (in press).

For the computation of carbon fluxes by fecal pellets of tunas, the average biomass has been computed including all the age classes of immature and mature tuna. The fishing impact is estimated by comparison of the average of the first (1980-1989) and last (2000-2009) decades of the time series (Fig. 5.4.5).

Impact of fishing on carbon sequestration by sinking fecal pellets

Method

Once the spatial distributions of tuna biomass is estimated (cf above), the carbon sequestration by daily production of fecal pellets can be computed using the Martin's curve for remineralization. The Martin Curve is an empirical power-law model that describes how particulate organic carbon (POC) flux decreases with ocean depth due to remineralization and dissolution processes (Martin et al. 1987). This curve can be applied to the tuna fecal pellets that are contributing to the POC and can be expressed as follows:

$$F(z) = C_u \left(\frac{z}{z_{ref}} \right)^{-k}$$

With *F(z)* is the remaining flux of carbon at depth *z*, C_u the unassimilated carbon contained in the fecal pellets, z_{ref} the reference depth where the initial flux is measured or estimated and *k* the attenuation coefficient, estimated to 0.858 in Martin et al (1987). Sinking organic carbon becomes effectively sequestered for centuries from the atmosphere once it descends below the permanent pycnocline (~1,000 m depth), a layer of stable density in the ocean which is also the boundary between mesopelagic and bathypelagic ecosystems. Therefore, the remaining carbon flux is estimated at depth z = 1000 m.

A standard value used for the wet weight to carbon ratio is 0.15, based on a dry weight to wet weight ratio of 0.3 and a dry weight carbon content of 50%. There are a few estimates of the daily food ration of tuna. Olson & Mullen (1986) measured daily food intake of eastern Pacific yellowfin tuna based on several methods. They found a mean daily food ration of 3.9% body weight/day using gastric evacuation, 5.2% based on bioenergetics estimates and 6.7% based on cesium concentrations. While the food ration varies with size, it can be set to an average of 5% of the body weight. Therefore, the daily unassimilated carbon (C_{exc}) can be estimated based on the biomass of tuna as:

$C_{exc} = r \ c \ B$

With B the biomass, r the daily food ration (r=0.05), and c the conversion factor from wet weight to carbon (c= 0.15).

While sinking after being excreted, feces start to be remineralised by bacteria and zooplankton. The Martin curve (1987) is an empirical power-law model that describes how the flux of sinking particulate organic carbon (POC) decreases with depth:

$$F(z) = F_{z_0} \left(\frac{z}{z_0} \right)^{-b}$$

With *F(z)* the POC flux at depth z; F_{z0} the POC flux at reference depth Z_0, and b the attenuation coefficient (commonly 0.858). The curve shows that most remineralisation occurs within the upper few hundred meters of the ocean. For tuna, it can be assumed that most excretion takes place in the epipelagic layer. This is either because they spend the majority of their time in this layer—as is the case for skipjack and small-sized yellowfin and bigeye tuna—or because, even when they dive into the mesopelagic zone to hunt prey (as bigeye tuna often do), they return to the warmer waters of the epipelagic layer to recover. It is likely that most digestion also occurs in this upper layer, where higher temperatures enhance physiological processes.

Therefore, Martin curve can be applied to the carbon excreted by the total biomass at a mean depth of eg., 50 m to estimate the remaining carbon that is not remineralized at 1000 m and would then be sequestered for several decades to centuries. The result can be provided as spatial distribution in gC m2 (Figure 5.4.6a) or integrated over the domain in multiplying the mean

abundance (g/m2 or t/ km2) by the surface area of the cells accounting for latitude correction (Figure 6b). The impact of fishing on carbon sequestration at 1000m can be computed by difference between the biomass estimated with and without fishing (Figure 5.4.7). The total average flux by species with and without fishing and the average distributions have been computed and are provided as csv and NetCDF files (see Description of data set).

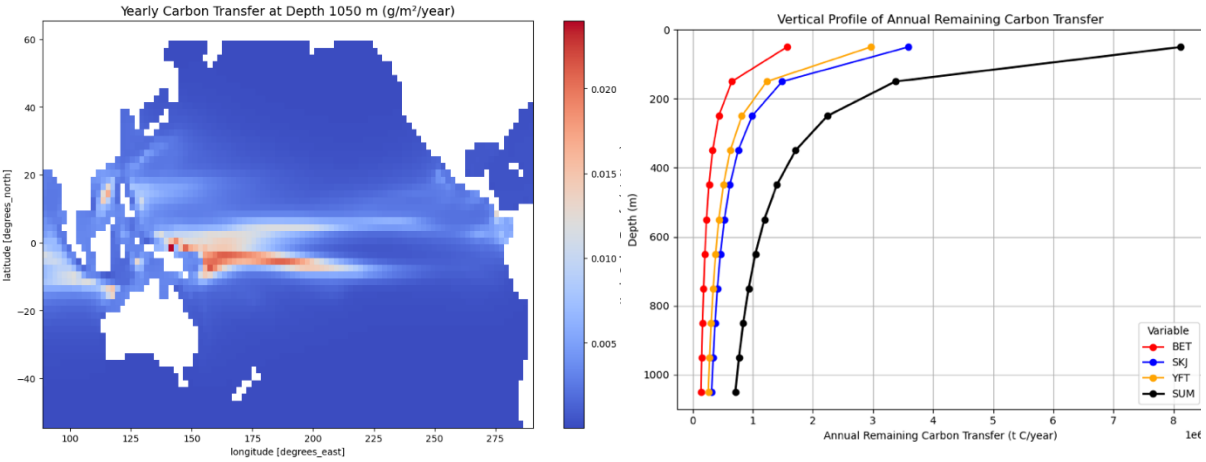

Figure 5.4.6. Contribution of tuna excretion (feces) to the vertical carbon flux in absence of fishing. (a) Estimation of mean annual distribution of carbon transfer at 1000 m depth for the Pacific skipjack stock; (b) depth profiles of mean annual carbon transfer by species and total of species.

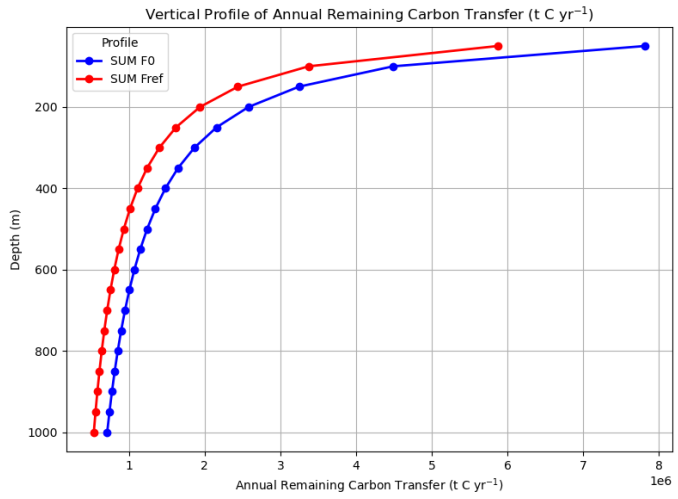

Average Carbon flux at 1000 m by main Pacific tropical tuna species (tC yr^{-1})

Bigeye	Without fishing	142
		292
Skipjack		326
		403
Yellowfin		242
		525
Bigeye	With fishing	96 949
Skipjack		272
		108
Yellowfin		165
		294

Figure 5.4.7. Impact of fishing on the carbon flux from fecal pellets by the three main tropical tuna species in the Pacific, in average over the period 1980-2010.

Impact of fishing on carbon sequestration due to tuna deadfall

Industrial fisheries impact carbon sequestration by removing tuna bodies that therefore did not sink to the deep ocean. The carbon of fished tuna carcasses is reemitted to the atmosphere in a relatively short time, except for the bones which represent 6% of the biomass (Garrido Gamarro et al., 2013; Nicholson, 1998). The fishing mortality impacts the young immature and adult tunas. We provide the total biomass by species being the sum of young and adult cohorts under a reference scenario (Fref) that includes the historical fishing and the same total biomass estimated in absence of fishing (F0). The impact of fishing on carbon sequestration by tuna deadfall can be estimated by the difference between these two simulations (F0-Fref) using the files provided (see appendix). To convert wet weight biomass in carbon, we considered that each individual tuna contains, on average, 12.5 ± 2.5% of carbon in its fresh biomass (Bar-On et al., 2018; Czamanski et al., 2011).

Fuel consumption and CO2 emission

Parker etal (2018) have estimated that fisheries consumed 40 billion litres of fuel in 2011 and generated a total of 179 million tonnes of CO_2-equivalent GHGs (4% of global food production). Emissions from the global fishing industry grew by 28% between 1990 and 2011, driven primarily by increased harvests from fuel-intensive crustacean fisheries. In recent years, tuna fisheries extracted globally an annual average of ~7 million tons, with the Pacific Ocean accounting for around 74% of the total (FAO, 2020). The tuna fishing industry also relies heavily on fossil fuel for vessel propulsion and onboard energy, especially for the freezing process. Note that freezing makes slower transportation possible allowing less fuel consumption for transport. Therefore, an optimization between these two sources of energy consumption is possible.

Based on a large survey representing a total of 199 vessels in three oceans, using four main fishing gears, Tyedmers and Parker (2012) estimated the combustion of fuel and associated CO2 emitted in the atmosphere according to the fishing methods (Table 5.4.1). Fuel-specific GHG emissions, as well as emissions associated with upstream production of fuel were converted into carbon dioxide-equivalent emissions (CO2-e) using IPCC (2007) characterization factors. The resulting life cycle average GHG emission intensity of fuel was 3.12 kg CO2-e per litre of fuel burned.

The results showed a marked difference in fuel use intensity between tuna fisheries targeting primarily skipjack and yellowfin tuna with purse seine, and those targeting albacore, bigeye and bluefin tuna with longline, troll, and pole and line gears. The former group, using purse seine gear, was found to burn, on average, 368 litres of fuel per live weight tonne of landings, emitting 1,148

KG of CO2e, while the latter group of fisheries using other gears was found to burn, on average, between 1069 (longline) and 1485 (pole and line) litres per tonne, with corresponding emission of 3,335 and 4,633 KG CO2e, respectively.

Using these estimates, it is possible to calculate the mean fuel consumption and CO2-equivalent emission for each tonnes of tuna catch.

Table 5.4.1. From Tyedmers and Parker (2012). Average 2009 fuel use intensities (FUI in litre per tonne of landing) of vessel reporting aggregated by ocean, species and gear for data collection.

Landings reported (tonnes)		FUI (L/ t)	CO2e (KG/t)
Atlantic Ocean	67,899	513	1,601
Indian Ocean	62,497	454	1,416
Pacific Ocean	669,527	354	1,104
Purse seine	793,858	368	1,148
Longline	453	1,069	3,335
Troll	1,464	1,107	3,454
Pole and line	4,148	1,485	4,633
Albacore	5,411	1,303	4,065
Bigeye	28,339	465	1,451
Bluefin	860	1,478	4,611
Skipjack	655,886	364	1,136
Yellowfin	109,427	395	1,232
All tuna	799,923	375	1,170

Description of data set

Accessible on google drive:
https://drive.google.com/drive/folders/1nHHwOz3xQOYyC2X1kpVZrgaPWDfhFswd?usp=drive_link

Variable	File name	Variable name	Unit
Pacific Micronekton			
Epipelagic resident biomass	B_mnk_d1_n1.nc	B_mnk_d1_n1	g WW m^{-2}
Upper migrant mesopelagic biomass	B_mnk_d2_n1.nc	B_mnk_d2_n1	g WW m^{-2}
Upper resident mesopelagic biomass	B_mnk_d2_n2.nc	B_mnk_d2_n2	g WW m^{-2}
Lower highly migrant mesopelagic biomass	B_mnk_d3_n1.nc	B_mnk_d3_n1	g WW m^{-2}
Lower migrant mesopelagic biomass	B_mnk_d3_n2.nc	B_mnk_d3_n2	g WW m^{-2}
Lower resident mesopelagic biomass	B_mnk_d3_n3.nc	B_mnk_d3_n3	g WW m^{-2}
Pacific Skipjack			
Biomass total Fishing	skj_Btot_hist_Fref.nc	skj_Btot	g WW m^{-2}
Biomass total No fishing	skj_Btot_hist_F0.nc	skj_Btot	g WW m^{-2}
Mean annual distribution of carbon transfer at 1000 m depth by skipjack feces in absence of fishing	Yearly_carbon_transfer_at_1000m_skj_F0.nc	carbon_at_depth_1000m	g C m^{-2} yr^{-1}

	Mean annual distribution of carbon transfer at 1000 m depth by skipjack feces with historical fishing	Yearly_carbon_transfer_at_1000m_skj_Fref.nc	carbon_at_depth_1000m	g C m^{-2} yr^{-1}
	Total average annual carbon flux at 1000m by skipjack in absence of fishing	Annual carbon flux_1000m_F0_skj.csv	annual_remaining_carbon_tC_year	t C yr^{-1}
	Total average annual carbon flux at 1000m by skipjack with fihing	Annual carbon flux_1000m_Fref_skj.csv	annual_remaining_carbon_tC_year	t C yr^{-1}
Pacific Yellowfin				
	Biomass total Fishing	yft_Btot_hist_Fref.nc	yft_Btot	g WW m^{-2}
	Biomass total No fishing	yft_Btot_hist_F0.nc	yft_Btot	g WW m^{-2}
	Mean annual distribution of carbon transfer at 1000 m depth by yellowfin feces in absence of fishing	Yearly_carbon_transfer_at_1000m_yft_F0.nc	carbon_at_depth_1000m	g C m^{-2} yr^{-1}
	Mean annual distribution of carbon transfer at 1000 m depth by yellowfin feces with historical fishing	Yearly_carbon_transfer_at_1000m_yft_Fref.nc	carbon_at_depth_1000m	g C m^{-2} yr^{-1}
	Total average annual carbon flux at 1000m by yellowfin in absence of fishing	Annual carbon flux_1000m_F0_yft.csv	annual_remaining_carbon_tC_year	t C yr^{-1}
	Total average annual carbon flux at 1000m by yellowfin with fishing	Annual carbon flux_1000m_Fref_yft.csv	annual_remaining_carbon_tC_year	t C yr^{-1}
Pacific Bigeye				
	Biomass total Fishing	bet_Btot_hist_Fref.nc	bet_Btot	g WW m^{-2}
	Biomass total No fishing	bet_Btot_hist_F0.nc	bet_Btot	g WW m^{-2}
	Mean annual distribution of carbon transfer at 1000 m depth by yellowfin feces in absence of fishing	Yearly_carbon_transfer_at_1000m_bet_F0.nc	carbon_at_depth_1000m	g C m^{-2} yr^{-1}
	Mean annual distribution of carbon transfer at 1000 m depth by yellowfin feces with historical fishing	Yearly_carbon_transfer_at_1000m_bet_Fref.nc	carbon_at_depth_1000m	g C m^{-2} yr^{-1}
	Total average annual carbon flux at 1000m by yellowfin in absence of fishing	Annual carbon flux_1000m_F0_bet.csv	annual_remaining_carbon_tC_year	t C yr^{-1}
	Total average annual carbon flux at 1000m by yellowfin with fishing	Annual carbon flux_1000m_Fref_bet.csv	annual_remaining_carbon_tC_year	t C yr^{-1}

Simulations with FEISTY

Model description

FEISTY (FishErIes Size and functional TYpe model) models the entire fish community and includes a simple model of the benthos. FEISTY model is designed to be mechanistic, simple and fast, generally applicable globally, and compatible with biogeochemical model principles. It is based on ordinary differential equations and careful accounting of mass balancing with a production-constrained one-way coupling to the LTL models. FEISTY does not resolve specific fish species but structures the fish community around a few functional types (aka. functional groups or guilds) based on traits of asymptotic size and feeding strategy in the vertical water column (pelagic, demersal, or mesopelagic). This simplification, together with the mechanistic basis, allows for projections into novel environments, e.g., climate change projections.

FEISTY have previously been developed to use in a global environment (Petrik et al. 2019; van Denderen et al. 2021). Within NECCTON it has been implemented as an efficient Fortran library with an R front-end (Zhao et al. 2025). Further, we have derived global fisheries exploitation rates and validated the model (Van Denderen et al. 2024). To be able to couple FEISTY to time-varying forcing from the LTL models, we have also implemented a time-varying input forcing option. Within NECCTON we are testing the hypothesis that we can also model fish communities on a regional scale *without changing model parameters between regions*. The only parameters changed are the two ecological efficiencies that are used to couple the zooplankton and benthic productions to each LTL model.

Model Formulations: State Variables, Equations, Parameters

The biological basis of FEISTY is described in the publication Zhao et al (2024), with a concise description of all equations and parameters in the vignette for the R-package. Here we will therefore mainly describe the developments that are go beyond this description: the time-varying input and the coupling to the LTL models.

First, we provide a brief overview of FEISTY (this is a verbatim copy of the “methods section” in Zhao et al, 2025). For full details, including equations and parameters, please access the vignettes in R after installing the package: `browseVignettes("FEISTY")`.

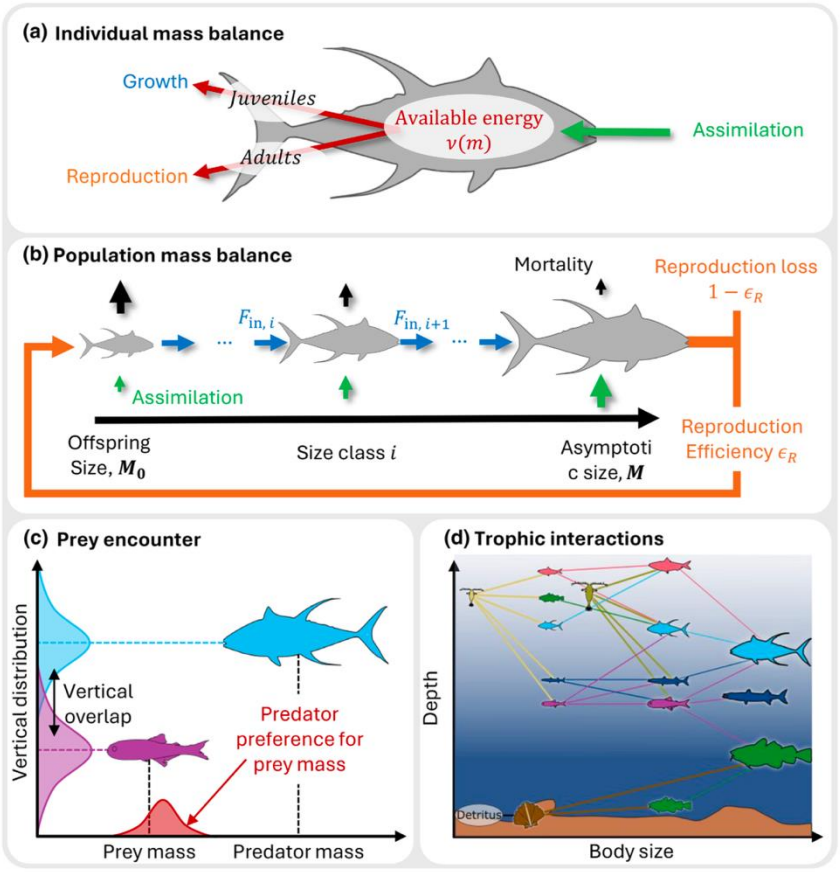

Figure 5.4.8. Sketch of the FEISTY framework. (a) Individual mass balanced allocation of energy of a fish. (b) Population mass balance of a fish functional type. (c) An example of a prey encounter between two functional types where a large fish (blue) eats a smaller prey (purple) when their vertical distributions overlap. (d) Schematic representation of trophic interactions between functional types emerging from the size and vertical interactions. The full model encompasses three resources: small and large mesozooplankton (sand color), a benthic resource (brown), and five functional types: small and large pelagics (pink and cyan), demersal fish (green), mesopelagic fish (purple), and midwater predators (blue).

FEISTY is similar to other size-based fish models by representing the processes of competition and predator-prey interactions that emerge from larger fish feeding on smaller fish that share the same habitat. In contrast to most fish food web models, it abstains from representing specific species in favor of grouping species into functional types, i.e., small and large pelagic fishes, demersal fish, mesopelagic fish, and midwater predators. The description removes the requirement of having a species-specific representation of density dependence between spawning biomass and recruitment, the traditional “stock-recruitment” relationship used in fisheries science, which was a hindrance to properly representing the influence of the secondary production on the fish community. Loss processes, e.g., resource competition and mortality, that affect the larval and juvenile stages are here explicitly represented instead of imposing an external carrying capacity on each functional type.

All processes in FEISTY are described at the level of an individual fish that is defined by its body size (mass) m and is affected by temperature. The core is a mechanistic description of the individual's energy budget (Figure 5.4.8a above). Prey are consumed based on encounter rates, consumed food is

assimilated and respired, and the remaining available energy is divided between growth and reproduction according to the maturity of the fish.

Individual-level processes are scaled to the population level of each functional type. A functional type is characterized chiefly by its maximum (asymptotic) mass and its vertical feeding habitat (Figure 5.4.8b and c).

Fish are spawned at their offspring size (1 mg) and use their available energy to grow through each size class. Somatic growth leads to a flux of biomass between size classes. Mature fish allocate energy to reproduction and that defines the flux of new offspring that is routed back to the smallest size (Figure 5.4.8b).

The main governing equation is a discretization of the McKendric-von Foerster equation for mass balanced growth. The equation describes the change of biomass in a size class due to the flux between neighbouring size classes and the accumulation and loss of biomass due to somatic growth, reproduction, and mortality:

$$\frac{\mathrm{d}B_i}{\mathrm{d}t} = J_i - J_{i+1} + (\nu_i - \rho_i - \mu_i)B_i,$$

With B_i being the biomass (units of biomass per area) in the th size class, J_i and J_{i+1} are the fluxes of biomass in and out of the size class i (units of biomass per area per time), ρ_i is the biomass-specific reproduction rate (units of per time), and μ_i is the biomass-specific mortality rate (units of per time). ν_i represents the biomass-specific energy acquired from predation on the resources or fish (units of per time) after accounting for basal metabolism, which is used for increasing the biomass and for reproduction ρ_i in the adult size classes.
Fish interact with other size-classes through predation following the principle that big fish eat smaller fish in a shared habitat, such that the feeding preference (dimensionless) between a predator size class i and a prey size class j (including mesozooplankton and benthic resource) is:

$$\theta_{i,j} = \theta_{\mathrm{size},i,j}\,\theta_{\mathrm{vertical},i,j},$$

where, θ_{size} represents the size-based feeding preference and $\theta_{vertical}$ represents the vertical overlap between the predator and prey (Figure 5.4.8c).

Predation fuels growth and reproduction of the predator while also imposing predation mortality on the prey. These feeding interactions, together with the bioenergetic model, define fluxes in and out of size class , the available energy for growth, the reproduction rate, and the mortality.

Benthos

Due to the limited access to benthos biomass in the NECCTON LTL models, the benthos community is modelled as logistic growth according to time-varying production and limited by a carrying capacity:

$$\frac{\mathrm{d}R}{\mathrm{d}t} = r(t)\left(1 - \frac{R}{K}\right)R - \sum \mu_{\mathrm{R}\,i} R,$$

where *r(t)* is the benthos production given as the detritus flux towards the seabed and $\mu_{R\,i}$ is the mortality by fish eating on the benthos.

https://github.com/Kenhasteandersen/FEISTY

Simulation setup

In FEISTY the fishing scenarios are no fishing and fishing with a fishing mortality of 0.5/yr on large pelagic fish. The fisheries selectivity is implemented on fish larger than 5 kg. Flux to the sea-bed is calculated from the fecal pellet fluxes from the fish discounted by a Martin curve.

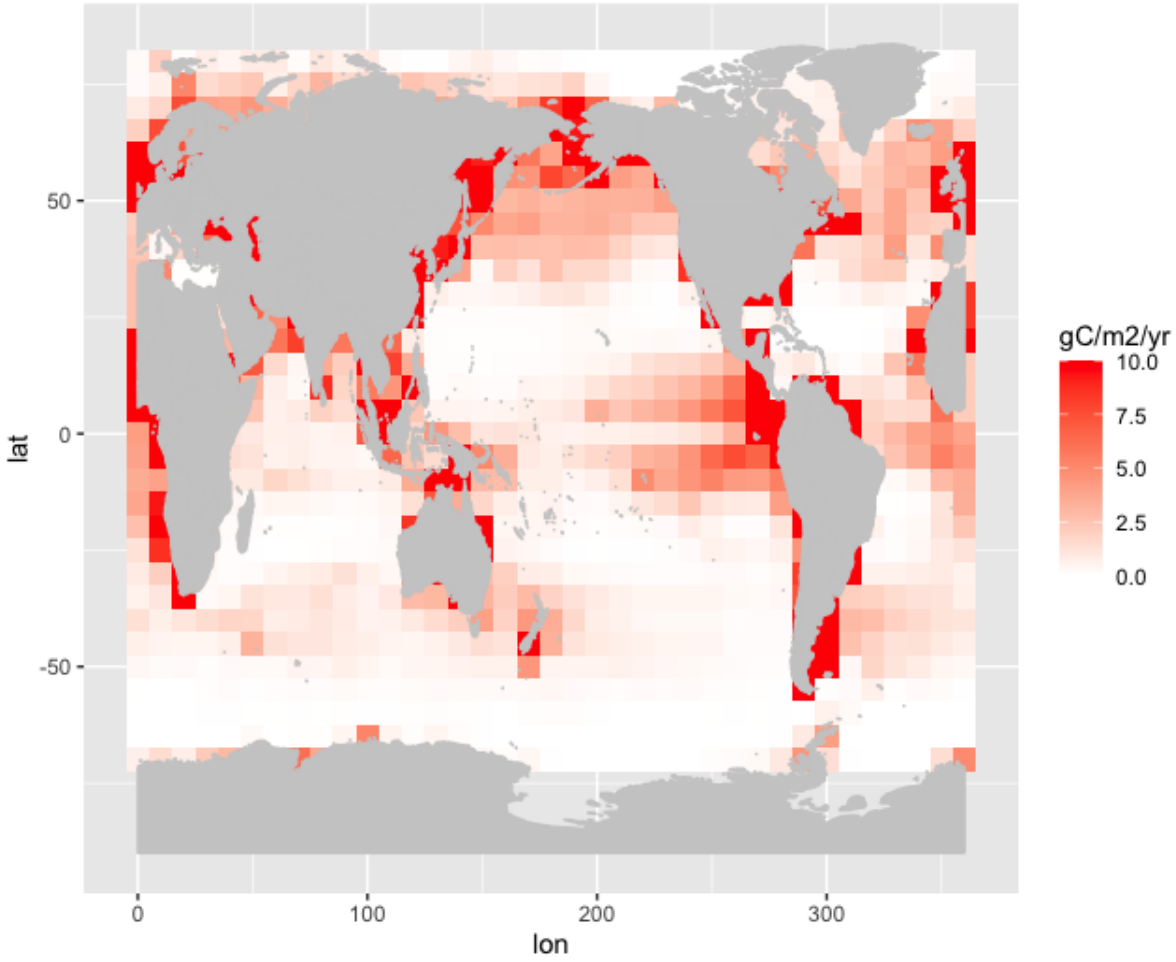

Figure 5.4.9. Results of simulations with FEISTY. It shows the flux of carbon the seabed in a situation without fishing.

Simulations with FEISTY shows rates of fecal pellet fluxes to the seabed in the range of 0-10 g carbon/m^2/yr, largest in shelf ecosystems and along the equatorial upwelling, and smallest in the oligotrophic gyres (Figure 5.4.9).

Adding fishing generally *reduces* the carbon flux to the seabed (Figure 5.4.10). The reduction is generally in the order of 0-0.5 g carbon/m^2/yr, i.e., roughly around 10%. This means that the hypothesis that the increase in forage fish due to the predatory release from the reduction in large pelagic fish is insufficient to compensate for the reduced carbon flux due to the reduction in large pelagic stocks. Fishing therefore reduces the carbon sequestration.

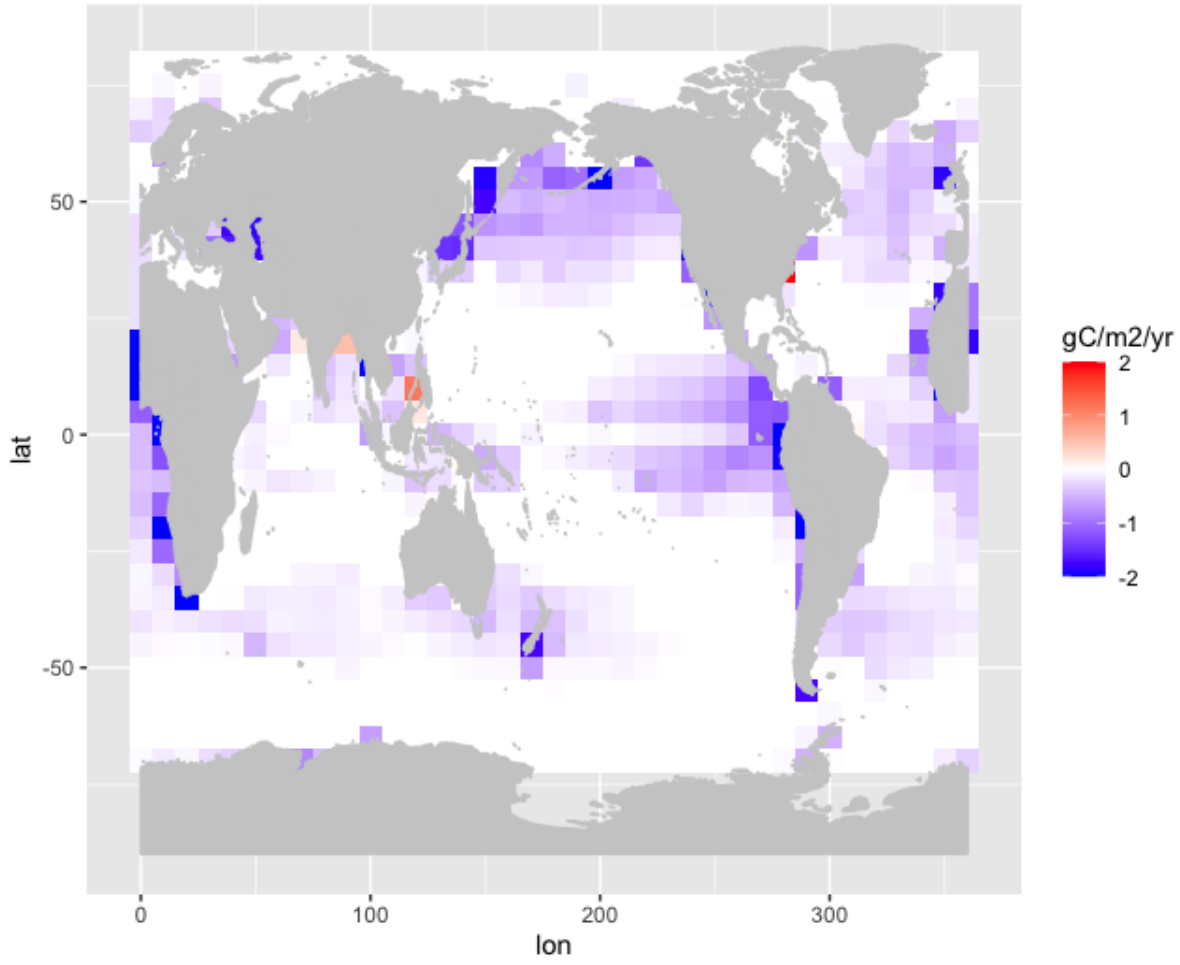

Figure 5.4.10. Change in carbon flux to the seabed due to fishing on large pelagic fish with a fishing mortality of 0.5/year.

Description of data set

The dataset is in the format of an R data file and contains the variables:

- `lat, lon`: latirude and longitude
- `Jbottom, JbottomF`: flux to the bottom without and with fishing on large pelagics in units of $gC/m^2/yr$.

The dataset is hosted on Zenodo: https://doi.org/10.5281/zenodo.15718757

Contribution to the overall objectives and relevant (KPIs)

As described in this deliverable, the work and results contribute to the following scientific and technical objectives:
ST1 Explore the role of key organisms across basin scales and quantify the past, current and future state of the ocean C cycle, with a particular focus on the BCP.
ST4 Develop a suite of tools to predict the impact of resource extraction processes on the contemporary ocean C cycle, the optimal measurement of the Ocean C cycle and build Decision Support Tools (DSTs) to predict the impacts of industrial processes in a future ocean.

This deliverable will also be used to contribute to the following KPIs:
(22) Managers in fishing industry aware of impact on C and integrating this into their planning
(23) Managers in industry aware of impact on C and including this in their forward planning
(27) Managers in fishing and other industries, & policymakers in coastal states aware of their impact on C and integrating this into their planning
This will be done through the DSTs, but also by presenting results of the simulations to the relevant stakeholders.

Impact and progress beyond state of the art

Task 5.1: Impacts of deep seabed mining and drilling activities on the open ocean

The preliminary pelagic model results indicate that impacts become stronger the closer the sediment discharge occurs to the sea surface and the longer the

discharge time in a certain area is. The main effect occurs in the euphotic zone due to an increase in light attenuation and therefore light limitation for the phytoplankton growth including subsequent effects on the biogeochemical turnover. However, it should be noted that our sensitivity experiments are currently only 1D and that not all relevant processes have been investigated (e.g. different sediment discharge rates and particle aggregation and scavenging). Also, MOPS is a rather simple-structured biogeochemical model, which may not be able to appropriately reproduce the ecosystem structure at larger water depths. Therefore, potential impacts in deeper zones may not be predicted well. In this light we thus might have to consider continuing the investigation of waste sediment discharge with other models being able to represent ecosystem structure (such as ERSEM) and/or higher-trophic level (like fish model FEISTY) better. Since there are remaining gaps in data and knowledge regarding the ecosystem specifically in the Clarion-Clipperton Zone of the Pacific Ocean the main difficulty is nonetheless to parameterize and optimize these models for this region and habitat.

The benthic biogeochemical data and modelling indicate that biogeochemical processes, including organic carbon remineralization, in the sediment are severely impacted in the mining area and need thousands of years to recover to pre-impact conditions, essentially through build-up of the removed bioturbated layer by sedimentation of labile organic carbon (rates in the Clarion-Clipperton Zone are <0.5 cm/kyr).

Task 5.2: Impacts of sediment generating (e.g. dredging, trawling) activities on the shelf sea ecosystems

x

Task 5.3: Impacts of fishing on carbon sequestration in shelf ecosystem

In the Celtic Sea simulations, removing all fishing activities always resulted in a small decrease in carbon sequestration. By removing fishing pressure, guilds normally harvested are likely to reach higher biomass density resulting in higher food consumption and faeces production, boosting all food web interactions, especially within the water column. Consequently, CO_2 absorbed by the lowest trophic levels (phytoplankton and kelp) will have a longer lifetime in the system before seabed sequestration.

According to the Celtic Sea model outputs, benthos might play an important role in carbon sequestration. In future simulations, it would be interesting to

test other fishing scenarios to assess in more detail the role of benthos and seabed dynamics on carbon sequestration. Current ideas include selective fishing (e.g. no fishery of benthos), or isolating effect from fishing seabed disturbance by turning off catch but not the gear activities. Future work will also include simulations in other coastal regions available from the current list of StrathE2E implementations.

The N-to-C conversion algorithm allows for computation of annual carbon sequestration from StrathE2E nitrogen outputs. The difference with a simple Redfield conversion was significant but still very small. Work is on-going to improve the following two aspects of this first algorithm: (1) carbon equivalents to organic nitrogen decomposition processes (e.g. denitrification), and (2) representation of all DIC fluxes in the system.

The Ecopath modelling suggests that fishing has a limited, or even negligible, impact on the main carbon fluxes. This may be due to a weak top-down regulation in the Celtic Sea, as it has been highlighted for other marine systems. It should be stressed, however, that fishing as an economic sector is not limited to fish removal, but is a complex network relying on fuel consumption, refrigeration and transport, among many other energy-consuming activities.

Task 5.4: Impacts of fishing on carbon sequestration in off-shelf ecosystems

The method to estimate the carbon footprint of tropical tuna species has been developed and applied to key pacific species. The input datasets necessary to make these detailed estimates at a spatial resolution of 2 degrees are provided together with the outputs (see Description of data set). It is possible to measure the impact of fishing by difference between scenarios with fishing (Fref) and without fishing (F0). We are working in collaboration with other projects to improve and update the biomass estimates of tuna a increased resolution (1 degree) and also in the Indian and Atlantic Oceans. This first estimate of carbon flux could be then updated in the coming two years.

Lessons learnt and links built

Not applicable

References

Gascuel, D., Guénette, S., & Pauly, D. (2011). The trophic-level-based ecosystem modelling approach: Theoretical overview and practical uses. *ICES Journal of Marine Science*, *68*(7), 1403–1416. https://doi.org/10.1093/icesjms/fsr062

Acevedo-Gutierrez, A., Kennish, J. M., Levin, P. S., Lance, M. M., Jeffries, S. J., and Bromaghin, J. F. (2012) Isotope ratios of carbon and nitrogen from harbor seals and prey species analyzed at the Stable Isotope Core Laboratory in Pullman, WA in 2009 (Seal_response_to_prey project). Biological and Chemical Oceanography Data Management Office (BCO-DMO). (Version 04 December 2012) Version Date 2012-12-04. http://lod.bco-dmo.org/id/dataset/3708 [03/05/2025]

Artioli, Y., Katavouta, A., Holt, J., Harle, J., Galli, G., Mora, L., Merillet, L., and Conchon, A. (2023) "Deliverable 6.2 - 2020-2070 Future Projections (NEMO-ERSEM & SEAPODYM)." Mission Atlantic Project Report, WorkPackage 6 - Dynamics of ecosystem state; resources. www.missionatlantic.eu

Baker, C. A., Martin, A. P., Yool, A., & Popova, E. (2022). Biological carbon pump sequestration efficiency in the North Atlantic: A leaky or a long-term sink? Global Biogeochemical Cycles, 36, e2021GB007286. https://doi.org/10.1029/2021GB007286

Bar-On, Y. M., Phillips, R., & Milo, R. (2018). The biomass distribution on earth. Proceedings of the National Academy of Sciences, 115(25), 6506–6511.

Beauchard O, Soetaert K. Bottom fishing assessment tool: an R package to model the effects of bottom trawling on the marine benthos. Ecological Applications, under review

Bentley, J., Serpetti, N., Fox, C., Reid, D., Heymans, J., 2019. Modelling the food web in the Irish Sea in the context of a depleted commercial fish community. Part 2: ICES Ecopath with Ecosim Key Run. https://doi.org/10.13140/RG.2.2.15136.12809

Buesseler, K.O., Boyd, P.W., et al. (2007). Revisiting carbon flux through the ocean's twilight zone. Science, 316(5824), 567–570.

Callaway R, Engelhard GH, Dann J, Cotter J, Rumohr H (2007) A century of North Sea epibenthos and trawling: comparison between 1902–1912, 1982–1985 and 2000. Marine Ecology Progress Series 346:27–43

Clarke A (2008) Ecological stoichiometry in six species of Antarctic marine benthos. Marine Ecology Progress Series 369:25–37

Couce E, Schratzberger M, Engelhard GH (2020) Reconstructing three decades of total international trawling effort in the North Sea. Earth System Science Data 12:373–386

Czamanski, M., Nugraha, A., Pondaven, P., Lasbleiz, M., Masson, A., Caroff, N., Bellail, R., & Tréguer, P. (2011). Carbon, nitrogen and phosphorus elemental stoichiometry in aquacultured and wild-caught fish and consequences for pelagic nutrient dynamics. Marine Biology, 158(12), 2847–2862.

Gascuel, D., Guénette, S., & Pauly, D. (2011). The trophic-level-based ecosystem modelling approach: Theoretical overview and practical uses. ICES Journal of Marine Science, 68(7), 1403–1416. https://doi.org/10.1093/icesjms/fsr062

Gazis I.-Z., de Stigter H., Mohrmann J., Heger K., Diaz M., Gillard B., Baeye M., Veloso-Alarcón M.E., Purkiani K., Haeckel M., Vink A., Thomsen L., Greinert J. (2025) Monitoring benthic plumes, sediment redeposition and seafloor imprints caused by deep-sea polymetallic nodule mining. Nature Communications 16, 1229. DOI 10.1038/s41467-025-56311-0.

Guénette, Sylvie; Gascuel, Didier (2009). Considering both fishing and climate in a model of the Celtic Sea and the Bay of Biscay: what do we learn?. ASC 2009 - Theme session F. Conference contribution. https://doi.org/10.17895/ices.pub.25070990.v1

Guo, J., Brugel, S., Andersson, A., and Lau, D. C. P. (2022) Spatiotemporal carbon, nitrogen and phosphorus stoichiometry in planktonic food web in a northern coastal area. Estuarine, Coastal and Shelf Science, 272. https://doi.org/10.1016/j.ecss.2022.107903

Haffert L., Haeckel M., de Stigter H., Janßen F. (2020) Assessing the temporal scale of deep-sea mining impacts on sediment biogeochemistry. Biogeosciences 17, 2767-2789. DOI 10.5194/bg-17-2767-2020.

Hampton J., Lehodey P., Senina I., Nicol S., Scutt Philipps J., Tiamere K. (2022). Limited conservation efficacy of large-scale marine protected areas for Pacific skipjack and bigeye tunas. Frontiers in Marine Sciences. 9:1060943. https://doi.org/10.3389/fmars.2022.1060943

Heath, M. R., Speirs, D. C., Thurlbeck, I., and Wilson, R. J. (2021). StrathE2E2: An r package for modelling the dynamics of marine food webs and fisheries.

Methods in Ecology and Evolution, 12(2), 280–287. https://doi.org/10.1111/2041-210X.13510

Heath, M. R., and Speirs, D. C. (2023). StrathE2E2 version 4.0.1: Ecology model description. Department of Mathematics and Statistics, University of Strathclyde, Glasgow, UK. 13pp.

Heip C, Basford D, Craeymeersch JA, Dewarumez JM, Dorjes J, de Wilde P, Duineveld G, Eleftheriou A, Herman PMJ, Niermann U, Kingston P, Künitzer A, Rachor E, Rumohr H, Soetaert K, Soltwedel T (1992) Trends in biomass, density and diversity of North Sea macrofauna ICES Journal of Marine Science 49:13–22

Hernvann, P.-Y., Gascuel, D., Grüss, A., Druon, J.-N., Kopp, D., Perez, I., Piroddi, C., & Robert, M. (2020). The Celtic Sea Through Time and Space: Ecosystem Modeling to Unravel Fishing and Climate Change Impacts on Food-Web Structure and Dynamics. *Frontiers in Marine Science*, *7*, 578717. https://doi.org/10.3389/fmars.2020.578717

IPCC (Intergovernmental Panel on Climate Change) (2007). Climate change – The physical science basis. Contribution of Working Group I to the Fourth Assessment Report of the Intergovernmental Panel on Climate Change. New York: Cambridge University Press.

ISSF. 2025. Status of the world fisheries for tuna. Mar. 2025. ISSF Technical Report 2025-01. International Seafood Sustainability Foundation, Pittsburgh, PA, USA

Kerby TK, Cheung WWL, Engelhard GH (2012) The United Kingdom's role in North Sea demersal fisheries: a hundred year perspective. Reviews in Fish Biology and Fisheries 22:621–634

Koch, P. L., and McCarthy, M. D. (2016) Bulk Carbon and Nitrogen isotopes from sperm whale dentin from the UC-Santa Cruz labs of P. Koch and M. McCarthy (Sperm Whale SI Ratios project). Biological and Chemical Oceanography Data Management Office (BCO-DMO). Version Date 2016-08-01. http://lod.bco-dmo.org/id/dataset/652931 [03/05/2025]

König I., Haeckel M., Lougear A., Suess E., Trautwein A.X. (2001) A geochemical model of the Peru Basin deep-sea floor and the response of the system to technical impacts, Deep-Sea Research II 48, 3737-3756.

Martin, J.H., Knauer, G.A., Karl, D.M., & Broenkow, W.W. (1987). VERTEX: Carbon cycling in the northeast Pacific. Deep-Sea Research, 34(2), 267–285. https://doi.org/10.1016/0198-0149(87)90086-0

Moore B.R., Bell J.D., Evans K., Farley J., Grewe P.M., Hampton J., Marie A.D., Minte-Vera C., Nicol S., Pilling G.M., Scutt Phillips J., Tremblay-Boyer L., Williams A.J., N. Smith (2020). Defining the stock structures of key commercial tunas in the Pacific Ocean I: Current knowledge and main uncertainties. Fish. Res., 230, https://linkinghub.elsevier.com/retrieve/pii/S0165783620300424.

Moullec, F., Gascuel, D., Bentorcha, K., Guénette, S., & Robert, M. (2017). Trophic models: What do we learn about Celtic Sea and Bay of Biscay ecosystems? *Journal of Marine Systems*, *172*, 104–117. https://doi.org/10.1016/j.jmarsys.2017.03.008

Nicol S, Lehodey P, Senina I, Bromhead D, Frommel AY, Hampton J, Havenhand J, Margulies D, Munday PL, Scholey V, Williamson JE and Smith N (2022). Ocean Futures for the World's Largest Yellowfin Tuna Population Under the Combined Effects of Ocean Warming and Acidification. Front. Mar. Sci. 9:816772. doi:10.3389/fmars.2022.816772, https://www.frontiersin.org/articles/10.3389/fmars.2022.816772/full

Olson R.J. and Boggs C.H., (1986). Apex Predation by Yellowfin Tuna (Thunnus albacares): Independent Estimates from Gastric Evacuation and Stomach Contents, Bioenergetics, and Cesium Concentrations. Canadian Journal of Fisheries and Aquatic Sciences. 43(9): 1760-1775. https://doi.org/10.1139/f86-220

Parker, R.W.R., Blanchard, J.L., Gardner, C. et al. Fuel use and greenhouse gas emissions of world fisheries. Nature Clim Change 8, 333–337 (2018). https://doi.org/10.1038/s41558-018-0117-x

Petrik, Colleen M., Charles A. Stock, Ken H. Andersen, P. Daniël van Denderen, and James R. Watson. 2019. "Bottom-up Drivers of Global Patterns of Demersal, Forage, and Pelagic Fishes." Progress in Oceanography 176:102124.

Pitcher CR, Ellis N, Jennings S, Hiddink J G, Mazor T, Kaiser MJ, Kangas MI, McConnaughey RA, Parma AM, Rijnsdorp AD, Suuronen P, Collie JS, Amoroso R, Hughes KM, Hilborn R (2016) Estimating the sustainability of towed fishing-gear impacts on seabed habitats: a simple quantitative risk assessment method applicable to data-limited fisheries. Methods in Ecology and Evolution 8:472–480

Pitcher CR, Hiddink JG, Jennings S, Collie J, Parma AM, Amoroso R, Mazor T, Sciberras M, McConnaughey RA, Rijnsdorp AD, Kaiser MJ, Suuronen P, Hilborn R (2022) Trawl impacts on the status of biotic communities of seabed sedimentary habitats in 24 regions worldwide. Proceedings of the National Academy of Sciences of the United States of America 119:e2109449119

Potier, M., Savina-Rolland, M., Belloeil, P., Gascuel, D., & Robert, M. (2025). How will the cumulative effects of fishing and climate change affect the health and resilience of the Celtic Sea ecosystem? Science of The Total Environment, 969, 178942. https://doi.org/10.1016/j.scitotenv.2025.178942

Redfield, A. C. (1934) On the proportions of organic derivatives in sea water and their relation to the composition of plankton. In: James Johnstone Memorial Volume, edited by R.J. Daniel. Liverpool University press, Liverpool, UK, 176-192

Redfield, A. C. (1958) The biological control of chemical factors in the environment. American scientist, 46, 205-221

Redfield A. C., Ketchum B. H., and Richards, F. A. (1963) The influence of organisms on the composition of seawater. In: Comparative and descriptive Oceanography, edited by M. N. Hill. Wiley, New York, 26-77

Rynearson, T. (2019) Elemental carbon and nitrogen data for Skeletonema species as analyzed in Anderson and Rynearson, 2020. Biological and Chemical Oceanography Data Management Office (BCO-DMO). (Version 1) Version Date 2019-10-30. doi:10.1575/1912/bco-dmo.780386.1 [03/05/2025]

Salonen K, Sarvala J, Hakala I, Vilianen ML (1976) The relation of energy and organic carbon in aquatic invertebrate? Limnology and Oceanography 21:724–730

Scharler, U. M., Ulanowicz, R. E., Fogel, M. L., Wooller, M. J., Jacobson-Meyers, M. E., Lovelock, C. E., Feller, I. C., Frischer, M., Lee, R., McKee, K., Romero, I. C., Schmit, J. P., and Shearer, C. (2015) Variable nutrient stoichiometry (carbon:nitrogen:phosphorus) across trophic levels determines community and ecosystem properties in an oligotrophic mangrove system. Oecologia, 179(3), 863–876. https://doi.org/10.1007/s00442-015-3379-2

Schiettekatte, N. M. D., Barneche, D. R., Villéger, S., Allgeier, J. E., Burkepile, D. E., Brandl, S. J., Casey, J. M., Mercière, A., Munsterman, K. S., Morat, F., and Parravicini, V. (2020) Nutrient limitation, bioenergetics and stoichiometry: A new model to predict elemental fluxes mediated by fishes. Functional Ecology, 34(9), 1857–1869. https://doi.org/10.1111/1365-2435.13618

Senina I., Lehodey P., Hampton J., Sibert J. (2020b). Quantitative modeling of the spatial dynamics of South Pacific and Atlantic albacore tuna populations. Deep Sea Res. 175, 104667 https://doi.org/10.1016/j.dsr2.2019.104667

Senina I., Lehodey P., Sibert J., Hampton J., (2020a) Integrating tagging and fisheries data into a spatial population dynamics model to improve its

predictive skills. Canadian Journal of Aquatic and Fisheries Sciences, 77(3): 576-593, https://doi.org/10.1139/cjfas-2018-0470

Serpetti, N. (2012) Modelling and mapping the physical and biogeochemical properties of sediments on the North Sea coastal waters. PhD Thesis, University of Aberdeen. 249pp.

Sterner, R. W., and Elser, J. J. (2002). Chapter 8 – Big-Scale Stoichiometry: Ecosystems in Space and Time. In R.W. Sterner and J.J. Elser (Eds), Ecological stoichiometry: the biology of elements from molecules to the biosphere (pp. 313-369). Princeton University Press, Princeton, New Jersey.

Tyedmers, P. and R. Parker. 2012. Fuel consumption and greenhouse gas emissions from global tuna fisheries: A preliminary assessment. ISSF Technical Report 2012-03. International Seafood Sustainability Foundation, McLean, Virginia, USA

Van Denderen, P. Daniël, Colleen M. Petrik, Charles A. Stock, and Ken H. Andersen. 2021. "Emergent Global Biogeography of Marine Fish Food Webs." Global Ecology and Biogeography 30 (9): 1822–34.

Van Denderen, P. D., N. Jacobsen, K. H. Andersen, J. L. Blanchard, C. Novaglio, C. A. Stock, and C. M. Petrik. 2024. "Estimating Fishing Exploitation Rates to Simulate Global Catches and Biomass Changes of Pelagic and Demersal Fish." Earth's Future 12 (10). https://doi.org/10.1029/2024ef004604.

Van der Grient J.M.A, Drazen J.C. (2022) Evaluating deep-sea communities' susceptibility to mining plumes using shallow-water data. Science of the Total Environment 852, 158162. DOI 10.1016/j.scitotenv.2022.158162.

van der Reijden KJ, Eigaard OR, Bastardie F, van Denderen PD, O'Neill FG (2025) A gear component approach to trawling impact and sediment mobilization assessments. ICES Journal of Marine Science 82:fsaf106

Vanni, M. J., McIntyre, P. B., Allen, D., Arnott, D. L., Benstead, J. P., Berg, D. J., Brabrand, A., Brosse, S., Bukaveckas, P. A., Caliman, A., Capps, K. A., Carneiro, L. S., Chadwick, N. E., Christian, A. D., Clarke, A., Conroy, J. D., Cross, W. F., Culver, D. A., Dalton, C. M., … Zimmer, K. D. (2017) A global database of nitrogen and phosphorus excretion rates of aquatic animals. Ecology, 98(5), 1475. https://doi.org/10.1002/ecy.1582

Vink A. (2022) MANGAN 2021 Cruise Report: Independent scientific monitoring of two collector tests in the BGR and GSR contract areas for the exploration of polymetallic nodules in the equatorial NE Pacific. BGR cruise report, Bundesanstalt für Geowissenschaften und Rohstoffe, Hannover, Germany, 363 p. DOI 10.25928/hw7d-fs42.

Volz J. B., Haffert L., Haeckel M., Koschinsky A., Kasten S. (2020) Impact of small-scale disturbances on geochemical conditions, biogeochemical processes and element fluxes in surface sediments of the eastern Clarion-Clipperton Zone, Pacific Ocean. Biogeosciences 17 (4), 1113-1131. DOI 10.5194/bg-17-1113-2020.

Wilson, R. J., Speirs, D. C., Sabatino, A. & Heath, M. R. (2018) A synthetic map of the north-west European Shelf sedimentary environment for applications in marine science. Earth System Science Data, 10, 109-130.

Zhao, Yixin, Daniel van Denderen, Rémy Denéchère, Jonathan E. Falciani, Nis Sand Jacobsen, Themistoklis Konstantinopoulos, Daniel Ottmann, Colleen M. Petrik, Karline Soetaert, and Charles A. Stock. 2025. "FEISTY Fortran Library and R Package to Integrate Fish and Fisheries with Biogeochemical Models." Methods in Ecology and Evolution 16 (1): 40–48.